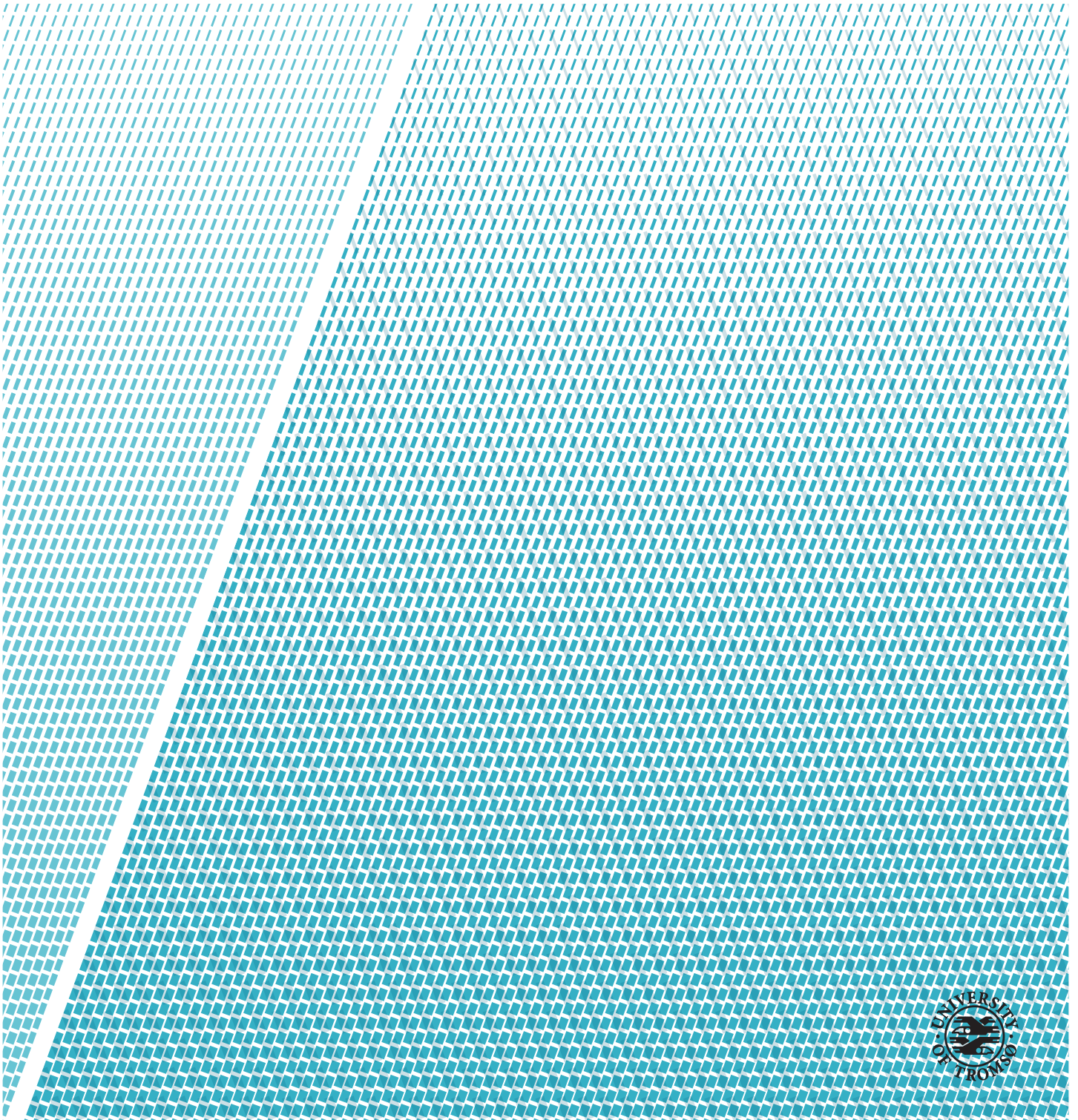


A Brief Look at the Performance of PV in Norway

Tobias Haumann

EOM-3901 Master's Thesis in Energy, Climate and Environment

December 2016



Abstract

In the past years the Norwegian PV market has grown substantially. The importance of data on how PV systems perform in Norway is therefore also increasing. In this thesis several Norwegian PV systems are analyzed mainly in terms of annual specific yields. The systems are located in western and southeastern Norway and near horizontal, tilted and vertical modules are looked at. Results show pretty similar performance of the near horizontal systems, so-called east/west applications, with 700 kWh/kWp being an approximate average annual specific yield. Vertical systems show large variations in yield due to shading losses and suboptimal orientations. Nonetheless, vertical systems having been placed well show great potential, having annual specific yields on the order of 700 kWh/kWp while producing far better than near horizontal systems in winter months.

Not surprisingly systems tilted 30° or more give the highest yields, slightly above 900 kWh/kWp seeming like a fair approximation for the annual specific yield of such systems in southern Norway. The measured yields have also been compared to estimated yield, giving a rough average deviation of 5%. Irradiation data from 57 locations in Norway has also been gathered, confirming that the average annual irradiation lies somewhere between 700 and 1000 kWh/m². The three irradiation models/databases Meteonorm 7.1, PVGIS and NASA SSE have been compared to this data by the means of RMS errors, indicating that Meteonorm and PVGIS perform similarly while the NASA database is less precise. Large local differences are observed though, making some models preferable in certain locations.

Simulations performed in PVsyst using average global and diffuse irradiation data from Trondheim, Bergen and Ås show that the increase in yield gotten from tilting a PV system varies not only with latitude but also the amount of diffuse irradiation at each location. Results indicate that the overall relative increase in yield gotten from tilting is the lowest in Bergen and highest in Ås, while the increase from tilting modules 10° is highest in Trondheim.

Acknowledgements

First off I would like to thank Monica Berner at Enova for taking the time to answer my questions and assisting with the structure of this thesis.

I am also grateful for the help and answers from Bjørn Thorud, Karl Andreassen, Arild Lunde and Christine Wangsnes. The irradiation data provided by Jan Olseth, Oddbjørn Grandum and Signe Kroken is also highly appreciated.

Lastly I want to thank Ingrid Beate for motivation and all the late dinners these past months.

Nomenclature

Acronyms

a-Si	Amorphous silicon
AM	Air mass
AOI	Angle of incidence
c-Si	Crystalline silicon
CdTe	Cadmium telluride
CIGS	Copper indium gallium selenide
DHI	Diffuse horizontal irradiance
DNI	Direct normal irradiance
FF	Fill factor
GHI	Global horizontal irradiance
IAM	Incidence angle modifier
LID	Light induced degradation
mono-Si	Monocrystalline silicon
MPP	Maximum power point
multi-Si	Multicrystalline silicon
NOCT	Normal operating cell temperature
POA	Plane of array
PV	Photovoltaic
STC	Standard test conditions

Symbols

α	Azimuth angle
β	Tilt angle
η	Efficiency
ω	Absorption coefficient of irradiation
ϕ	Solar zenith angle
θ	Angle of incidence
ζ	Solar altitude angle
b_o	ASHRAE IAM loss parameter
E_g	Band gap

$G_{t/h}$	Irradiance on a tilted/horizontal surface
I_{mp}	Maximum power point current
I_{sc}	Short circuit current
L	Latitude
U, U_c, U_v	Thermal coefficients
V_{mp}	Maximum power point voltage
V_{oc}	Open circuit voltage
W_p	Watt peak

Contents

Abstract	i
Acknowledgements	iii
Nomenclature	v
List of Figures	ix
List of Tables	xiii
1 Introduction and motivation	1
2 Photovoltaic theory and technologies	5
2.1 Solar irradiance and spectrum	5
2.1.1 Irradiance on a tilted surface	7
2.2 Efficiency of a solar cell	10
2.3 The main technologies today	12
2.3.1 Factors affecting efficiency and yield	14
2.4 PV orientation, yield and time of production	17
3 Simulations in PVsyst	21
4 Norwegian conditions for PV	25
4.1 Available data and the effect of the Norwegian climate on PV performance	25
4.2 Literature review of PV performance in Norway	29
5 System performance studies	31
5.1 Haakonvern ZEB, Bergen	31
5.2 Solsmaragden, Drammen	35
5.3 Grøndalen Gård, Auli	42
5.4 Powerhouse Kjørbo, Sandvika	46
5.5 Kiwi Fjeldset, Elverum	49
5.6 Other systems	53

5.6.1	Longyearbyen, Svalbard	53
5.6.2	"Låven" - Hedmark College, Evenstad	53
5.6.3	Oseana, Os	54
5.7	Summary	55
6	Sensitivity analyses	57
7	Conclusions and further work	65
A	The Perez Sky Diffuse Model	67
B	Average annual GHI for some locations in Norway	69
C	Tables of measured versus synthetic GHI/DHI	71
	Bibliography	75

List of Figures

1.1	Cumulative installed PV power in Norway, data from [20] and [21]	2
1.2	The turnkey price of residential, commercial and industrial PV systems in Norway, from IEA PVPS National Survey 2015 [20]	3
2.1	Standard AM0 and AM1.5 spectra, data from [6]	7
2.2	Solar angles and the angles of a tilted module, from [2]	8
2.3	The I-V and power curve of a solar cell/module, modified figures from [2]	11
2.4	The evolution of PV efficiencies, data from [5]	14
2.5	Effects of increasing irradiance and temperature on the I-V curve of a solar cell, from [2]	15
2.6	Spectral responses, from [48] and [15]	16
2.7	Illustration of shading effects on CIS modules, here by CIS manufacturer Solar Frontier [49]	17
2.8	Optimal tilt angles for different parts of the year, modified figure from [51]	18
3.1	Suggested albedo values from PVsyst	22
3.2	Spectral correction in efficiency as suggested by the Sandia Model for the mono-Si module SunPower SPR-225NE-WHT-D, modified figure from PVsyst	23
3.3	The default ASHRAE incidence angle modifier in PVsyst	24
4.1	Locations where irradiance data was available, red dots indicating data including both global aswell as direct and/or diffuse irradiance (base map by Kartverket)	26
4.2	Average monthly values of ground albedo at Fagklim, Ås 2009 - 2015 [40]	28
5.1	Part of the system at Haakonservern shortly after it's installation, photos: Arild Lunde	32

5.2	Expected and measured irradiation and yield, GHI measurements from eklima.no and yield data from sunnyportal.com .	33
5.3	2016 hourly precipitation at Flesland, data from eklima.no .	34
5.4	Average hourly power in comparison to a simulation based on 2016 irradiation and temperature data from Flesland (eklima.no)	35
5.5	The curved western facade and roof of Solsmaragden, photos from [31]	37
5.6	Some comparisons of monthly irradiation, yield and specific yields	39
5.7	An overview of Solsmaragden, colors indicating different inverters Original sketches gotten from Christine Wangsnes, Union Eiendom	40
5.8	Monthly and average hourly specific yields of the different parts of the Solsmaragden system	41
5.10	The eastern side of Solsmaragden showing the transformer close by, photos gotten from Christine Wangsnes, Union Eiendom and FUSen.no	42
5.9	Cumulative specific yield of the different parts of the Solsmaragden system, indicating snow on the roof in the period around 1/3 - 10/3	42
5.11	The PV system at Grøndalen Gård, photo: Karl Andreassen, Green Energy A/S	43
5.12	Monthly values of albedo used in the simulaton of the Grøndalen PV system	44
5.13	Measured and expected irradiation and yield, in addition to average monthly and hourly specific yields, POA irradiation data gotten from Karl Andreassen, Green Energy A/S	45
5.14	Average hourly specific yields at Grøndalen for each month, showing the shading effect	46
5.15	Part of the Powerhouse Kjørbo PV system, photo: Sigurd Øygarden Flåten	47
5.16	Measured and expected yield and irradiation at Powerhouse Kjørbo, measured GHI data from lmt.bioforsk.no	48
5.17	Monthly and average hourly specific yields of the different parts of the Powerhouse Kjørbo PV system	49
5.18	The roof and facade at Kiwi Fjeldset, photos from [37] and [38]	50
5.19	Expected and measured irradiation and yield at Fjeldset in addition to monthly and average hourly specific yields, dashed lines indicating periods with missing data. Measurements of GHI gotten from lmt.bioforsk.no	51
5.20	Cumulative specific yield at Kiwi Fjeldset	52
5.21	Part of the system at Longyearbyen and its monthly specific yield, photo and data gotten from Solbes AS	53

5.22	The roof mounted system at Evenstad and monthly its specific yield, photo by Statsbygg/Tove Lauluten and data from sunnyportal.com	54
5.23	Part of the Oseana system and its specific yield, photo by Aasa Christine Stoltz and data from sunnyportal.com	54
6.1	Monthly average irradiation at Trondheim, Bergen and Ås . .	58
6.2	Low-light efficiencies of the two modules used in the simulations	59
6.3	Annual specific yield results for different orientations at the three locations	61
6.4	The effect of irradiance levels and temperature, simulated at optimal tilt angles at each location with the Hay transposition model	62
6.5	Differences in monthly specific yield at Ås, using the Perez transposition model and two sets of monthly albedo values .	63
C.1	Average temperatures at Trondheim, Bergen and Ås, data from eklima.met.no	73

List of Tables

5.1	The system at Haakonsvern	32
5.2	Technical data on the SunForte PM096B00 module, from [28]	33
5.3	Technical data on the IBC MonoSol 280 ZX module, from [30]	36
5.4	Technical data on the ISSOL Cenit 220 Model 160, from IS-SOL presentation of Solsmaragden	37
5.5	The system at Solsmaragden	38
5.6	The system at Grøndalen Gård	44
5.7	Technical data on the Solar Frontier 165-S module, from [34]	44
5.8	Technical data on the SunPower SPR-327NE-WHT-D module, from [36]	46
5.9	The system at Powerhouse Kjørbo	47
5.10	The system at Kiwi Fjeldset	50
6.1	Technical data on the SunPower SPR-225NE-WHT-D module, from [36]	59
A.1	Intervals for ϵ bins	68
A.2	Coefficients for each ϵ bin	68
B.1	Gathered global horizontal irradiation data	69
C.1	Measured versus synthetic GHI and DHI at Gløshaugen, Trondheim	71
C.2	Measured versus synthetic GHI and DHI at Florida, Bergen .	72
C.3	Measured versus synthetic GHI and DHI at Fagklim, Ås . . .	72



Introduction and motivation

Although small when compared to others, the Norwegian PV market has begun to grow. Off-grid applications on cabins have been completely dominating the market up until recently. Accounting for over 80-90% of the market until 2015, this has been *the* way Norwegians have used PV until now. Other applications include the supply of lighthouses, lanterns and off-grid telecommunication stations, denoted as off-grid non-domestic applications here. Estimates for 2016 show that this is changing, though. Distributed grid-connected systems have begun contributing to the total installed power, as shown in figure 1.1. It should be noted that the numbers for 2016 in this figure are estimates from the consulting firm Multiconsult ASA; The biggest suppliers in Norway were asked what they expected to have installed within the year [21], giving an estimate of 6.14 MWp. As all of these suppliers have installed grid-connected systems only, an assumption of further stable growth in the off-grid market has been made, adding 100 and 700 kWp to the non-domestic and domestic market respectively.

About 95% of the electricity produced in Norway comes from hydropower. By early 2016 the installed power was just above 31 GW and the mean annual production 132 TWh [72]. With a typical annual consumption of electricity at about 120 TWh (ssb.no), the price of electricity in Norway is followingly lower than most countries in Europe [73]. As a result, the expected long term income

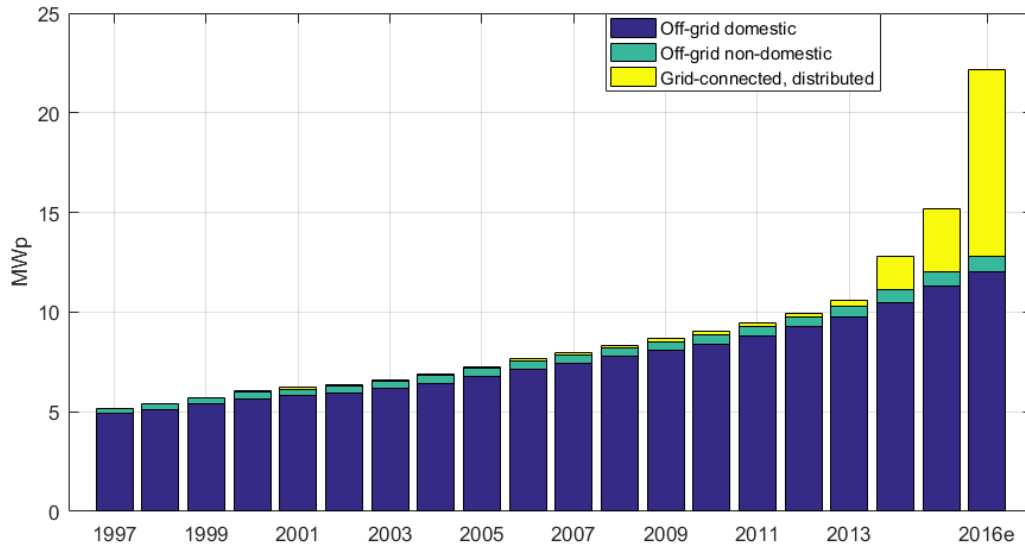


Figure 1.1: Cumulative installed PV power in Norway, data from [20] and [21]

of investing in a PV system in Norway has been low/nonexistent. With the price of PV coming down drastically in the last years, the competitiveness of solar energy will most likely be relevant for Norwegian customers in the coming years though. Economic incentives are also in place for those who consider PV in Norway. The municipality of Oslo will for example pay up to 40% of initial investments, while Enova SF can grant up to 10 000 NOK plus 1250 NOK per kWp for a PV system [74] [75].

The purpose of this thesis is thus to examine what yields can be expected of Norwegian PV systems by looking at measurements from systems installed within the past few years. The results are also to be compared with estimated yields, especially comparing sources of irradiation data. Lastly, simulations of different PV systems are performed using average weather data from the most densely populated areas in Norway as input.

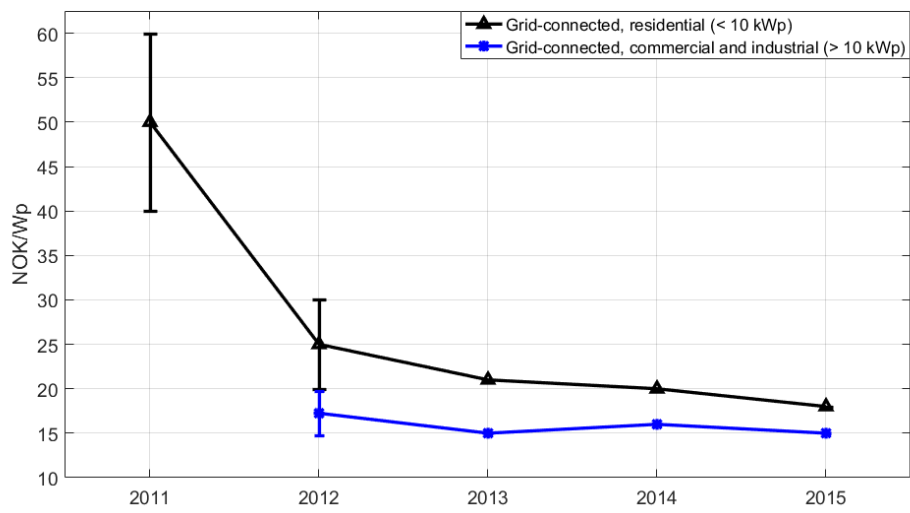


Figure 1.2: The turnkey price of residential, commercial and industrial PV systems in Norway, from IEA PVPS National Survey 2015 [20]

/2

Photovoltaic theory and technologies

The photovoltaic (PV) effect is the process in which photons, the packets of energy that make up electromagnetic radiation/light, is absorbed in a material and thereby excites electrons. The electrons are then lead through a load by a built-in electric field, and one has electric power. It was first reported by Edmond Becquerel in 1839 but did not become a research field of relative size until the 1970s, when non-fossil sources suddenly were relevant because of various oil embargos. Before this, space applications were the main usage [12]. Since then, research has lead to a handful of commercial technologies.

2.1 Solar irradiance and spectrum

The power of incoming solar radiation per unit area, given in W/m^2 , is also known as solar irradiance. Based on measurements from satellites, rockets, irradiance modelling and more the American Society for Testing and Materials has decided on a annual average value of $1366.1 \text{ W}/\text{m}^2$ for the extraterrestrial irradiance on a plane normal to the radiation, also known as the solar constant [2]. Irradiance integrated over a time period is known as the irradiation, usually given in kWh/m^2 . Once the solar radiation has reached the Earth's atmosphere some of it will be absorbed or scattered by atoms, molecules or

clouds. There are therefore two types of solar radiation reaching the Earth's surface: Direct and diffuse radiation. Direct radiation is defined as the radiation coming directly from the sun, and is followingly called beam radiation at times. Diffuse radiation, or sky radiation, is then the radiation a surface receives that comes from anywhere but directly from the Sun. When measuring irradiance, one usually distinguishes between global, direct and diffuse irradiance, global horizontal irradiance (GHI) being the sum of the horizontal direct and diffuse radiation:

$$GHI = G_{dir,h} + G_{diff,h} \quad (2.1)$$

The World Meteorological Organization suggests that the direct irradiance should be measured by looking at a 5° wide disk (2.5° half-angle) centered around the Sun [9]. Therefore, measured direct radiation includes both the radiation coming strictly from the Sun as well as a small portion of circumsolar radiation.

The spectrum of the average extraterrestrial solar radiation, showing how power is distributed among the wavelengths of the radiation, is shown as the graph labeled AM0 in figure 2.1, and the solar constant is gotten by integrating this spectrum over all wavelengths. AM0 refers to an air mass of 0, where air mass is a measure of how much atmosphere the solar radiation has to travel through. It is defined as $AM = 1/\cos(\phi)$, where ϕ is the zenith angle of the Sun [2]. The air mass is at its lowest when the Sun is directly overhead, giving $\phi = 0$ and $AM = 1$. AM0 is therefore just achievable at the top of the atmosphere. Both of the AM1.5 spectra in figure 2.1 represent radiation on a surface tilted 37° south.

Going through the atmosphere, there are several factors attenuating the solar radiation: Ozone layer thickness, amount of haze in the atmosphere/air (water vapour, dust particles, etc.) and the extent of the cloud cover [2]. The dips in the AM1.5 spectra in figure 2.1 are mainly due to absorption by aerosols and oxygen (O_2), ozone, water vapour and carbon dioxide [10]. In addition, there are mainly two types of scattering that occur in the atmosphere; Rayleigh scattering and Mie scattering. Generally, when the radiation meets particles smaller than its wavelength Rayleigh scattering occurs, while Mie scattering occurs when particles are equal to or larger than the wavelength. The scattered power as a result of Rayleigh scattering is dependent on the energy, and therefore also the wavelength, of the radiation or photons that it consists of. The energy of a photon is only dependent on its wavelength, given by the formula $E = hc/\lambda$, where E is the energy, h is Planck's constant, c is the speed of light and λ is the wavelength. It is actually inversely proportional to the fourth power of the wavelength, resulting in a much larger portion of the short wavelength, high energy, radiation being scattered this way [7]. Mie scattering is on the other hand not dependent on wavelength. This explains why clouds and fog which,

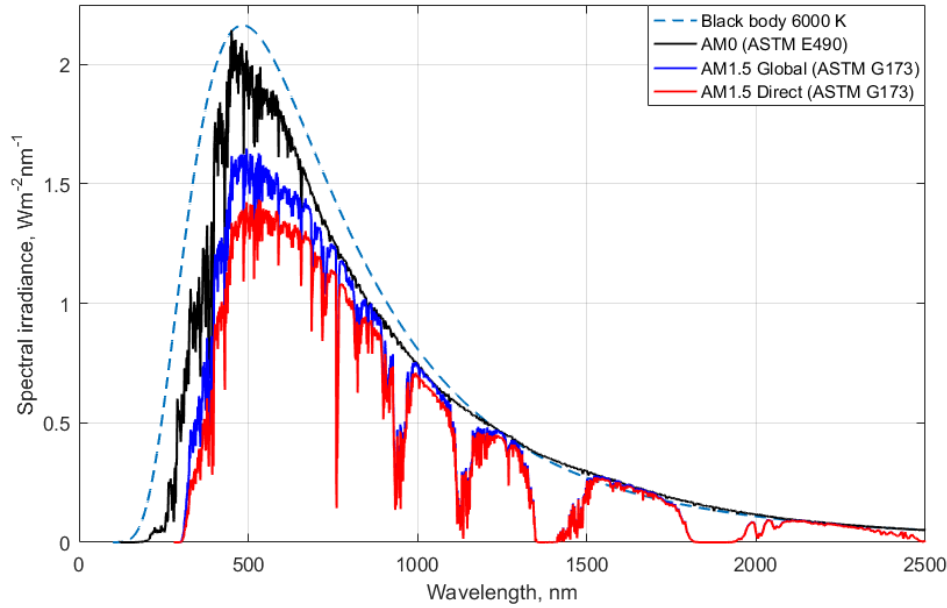


Figure 2.1: Standard AM0 and AM1.5 spectra, data from [6]

in contrast to most of the small molecules in the atmosphere, are made up of relatively large water droplets, appear white or grey. While the direction of scattered radiation as a consequence of Rayleigh scattering is spread pretty evenly in all directions, Mie scattering occurs mainly in the same direction as the incoming radiation. Because of this and the fact that blue light is on the short wavelength end of the visible spectrum, the sky is usually perceived as blue [11].

As the position of the Sun on the sky changes and different types of weather occur, it is then evident that the spectrum of incident irradiation as well as the ratio of direct/diffuse irradiation changes continuously and is dependent on location.

2.1.1 Irradiance on a tilted surface

It is often necessary to be able to go from measured/modeled horizontal irradiance to irradiance on a surface with a certain tilt and azimuth angle. The irradiance G_t hitting a tilted surface/module, or the plane of array (POA), can be divided into a direct, diffuse and ground-reflected component [16]:

$$G_t = G_{dir,t} + G_{diff,t} + G_{refl,t} \quad (2.2)$$

Given a direct normal irradiance (DNI) and GHI the direct and reflected component on a tilted surface can be expressed as

$$G_{dir,t} = \text{DNI} \cdot \cos(\theta) \quad (2.3)$$

$$G_{refl,t} = \text{GHI} \cdot \text{albedo} \cdot \frac{(1 - \cos\beta)}{2} \quad (2.4)$$

Here, the angle of incidence (AOI) θ is the angle between incoming direct radiation and the normal of the module, β is the tilt angle of the module and the albedo, or reflectivity, is chosen to be representative of the surrounding ground. The angle of incidence is given as [18]

$$\theta = \cos^{-1}((\cos\phi \cdot \cos\beta) + (\sin\phi \cdot \sin\beta \cdot \cos(\alpha_S - \alpha))) \quad (2.5)$$

where ϕ is the zenith angle of the Sun while α_S and α are the azimuth angles of the Sun and the plane of array respectively. North will be used as the 0° azimuth throughout this text, with east equal to the 90° azimuth and west the -90° or 270° azimuth. Using figure 2.2 as reference, the azimuth angles would be gotten by the relations $\alpha_S = 180^\circ + z$ and $\alpha = 180^\circ - Z_S$. The relation between the zenith angle and the elevation angle ζ of the Sun is $\phi = 90^\circ - \zeta$.

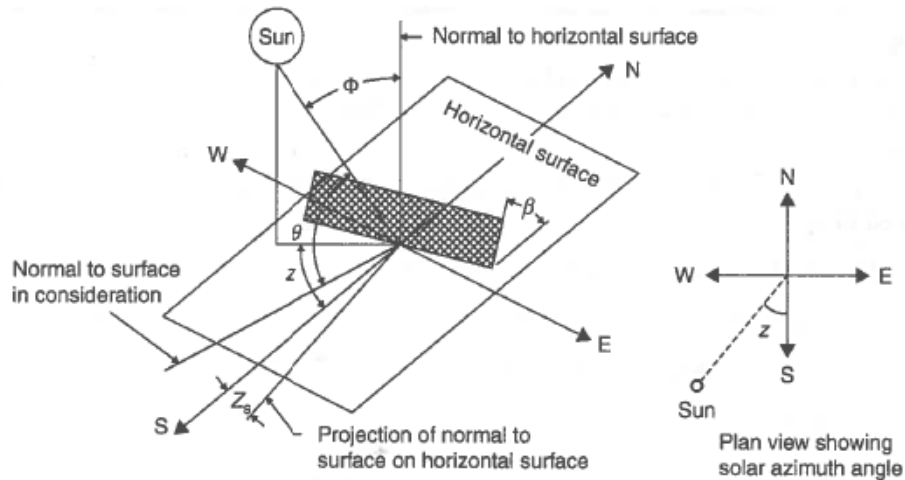


Figure 2.2: Solar angles and the angles of a tilted module, from [2]

If measurements of the diffuse horizontal irradiance do not exist, DHI can be calculated from GHI and DNI as

$$\text{DHI} = \text{GHI} - (\text{DNI} \cdot \cos(\phi)) \quad (2.6)$$

where the ideal cosine response of a pyranometer is included. A pyranometer's change of responsivity with varying zenith angle of the Sun is called its cosine

response [25], and applies to solar cells as well as other radiation sensors [27]. GHI can also be separated into DHI and $G_{dir,h}$ by the use of decomposition models. When DHI is known, the diffuse component on a tilted surface can be calculated using various transposition models. Models are often tuned to conditions of specific locations and the complexity of them varies: Some models assume an isotropic sky, meaning that the whole sky contributes equally to the amount of diffuse irradiance hitting the surface. The more complex models assume an anisotropic sky, taking into account that some parts of the sky contribute more than others. Maybe the simplest isotropic model gives POA diffuse irradiance as [44]:

$$G_{diff,t} = DHI \cdot \frac{(1 - \cos\beta)}{2} \quad (2.7)$$

Hay and Davies formulated a model which separates the diffuse irradiance into an isotropic and circumsolar component [45] as

$$G_{diff,t} = DHI \cdot ((A_i \cdot \cos(\theta)) + ((1 - A_i) \cdot \frac{(1 + \cos\beta)}{2})) \quad (2.8)$$

where A_i is an anisotropy index calculated as $A_i = DNI/G_{ex}$, G_{ex} being the extraterrestrial irradiance as calculated in appendix A. The Perez model separates the isotropic, circumsolar and horizon contributions and makes use of empirically determined coefficients to calculate the total diffuse component on a tilted surface. The set of equations and coefficients that are included in the model are given in appendix A while the diffuse component is calculated as follows [17]

$$G_{diff,t} = DHI \cdot (((1 - F_1) \cdot \frac{(1 + \cos\beta)}{2}) + (F_1 \cdot \frac{a}{b}) + (F_2 \cdot \sin\beta)) \quad (2.9)$$

There is also a transposition model tuned to Norwegian conditions, namely the Olseth and Skartveit model. Compared to 5 years of diffuse irradiance at various tilt angles in Bergen, it was found to fit well with data except for the case of a south-facing near vertical surface during winter months. It is basically an altered version of the Hay and Davies model and comprises of the following equations:

$$T_r = A_i \cdot \cos(\phi) \quad (2.10)$$

$$Y = 0.3 - 2T_r \quad (2.11)$$

$$G_{diff,t} = DHI \cdot ((A_i \cdot \cos(\theta)) + ((Y \cdot \cos(\beta)) + ((1 - T_r - Y) \cdot \cos^2(\beta/2))) \quad (2.12)$$

Here, T_r is the atmospheric transmittance of direct irradiance and Y is the fraction of the sky diffuse irradiance that originates from the zenith [46].

2.2 Efficiency of a solar cell

Solar cells can be made out of many different materials. In addition to being able to produce electricity by absorbing photons, they are all semiconductors. A semiconductor is a material that lies somewhere between an insulator and a conductor. The band gap of a material is important when categorizing materials in this way. The electrons surrounding the positively charged atom nucleus can be said to have a number of energy levels or bands where they can exist. The outermost band where electrons are present at absolute zero temperature, 0 Kelvin, is called the valence band, while the next available band is then called the conduction band. In insulators the energy gap between the valence band and the conduction band is large, making exciting electrons into the conduction band and thereby also the conduction of electricity difficult. This energy gap is called the band gap, E_g . Conductors have a very small band gap or none at all, while semiconductors lie somewhere inbetween [12].

The band gap of a solar cell material plays an important role in how efficient the cell eventually will be. The band gap is usually measured in electron-volts, eV, and represents the minimum energy needed to excite an electron to the conduction band. In solar cells this means that every photon with a wavelength corresponding to a lower energy than the band gap will not produce any electricity. One could then argue that a band gap as small as possible would result in the maximum amount of photons absorbed, but this is not the whole story. The band gap also dictates how much energy each excited electron can contribute to the load, as this, given by $q \cdot V_{mp}$, is always lower than E_g . Here q is the elementary charge of the electron and V_{mp} is the voltage of the cell at its maximum power point (MPP). Put in another way, a too small band gap limits the voltage the cell can produce, while a too large band gap limits the amount of photons that can excite charge and thereby the current it can produce [12]. For every solar spectrum there is therefore an optimal band gap. Shockley and Queisser discovered this in 1961, and came to the conclusion that the optimal band gap for a single junction cell was 1.1 eV, giving a theoretical maximum efficiency of 30% [13]. This calculation assumed the cell being illuminated by 6000 K black body, see figure 2.1, and that the cell held 300 K. One way to drastically improve the efficiency is to add types of materials with different band gaps to the cell structure, each separated by a new junction. This allows for a larger part of the incident spectrum to be absorbed without having to deal with losses accompanied with a too low photovoltage. Multi-junction cells (non-concentrating) have reached efficiencies of 38.8 % [5].

To transport the excited electrons through a connected load, there has to be an electric field built into the cell. This is done by doping one part of the material with elements that has one less electron in the valence band and the other part with elements that have one more. When connected, these then form

what is called a p-n junction. A voltage establishes across this junction and the cell essentially functions like a diode, letting current pass in one direction but blocking it in the other. This behavior gives solar cells their characteristic I-V curves, as shown in figure 2.3a, where the short circuit current I_{sc} and open circuit voltage V_{oc} are essential. As the names suggest, I_{sc} represents the current when the two sides of the p-n junction are connected with a small ohmic resistance, while V_{oc} is measured over the junction without connecting anything to the cell (infinite resistance) [2]. As the power output from a cell, module or array is given by the product of the current and the voltage, or $P = V \cdot I$, every cell has a point on the I-V curve where it produces maximum power, the MPP. Solar cells are sensitive to the resistance, or impedance, that they "see" at their terminals. Maximum power output is achieved when the resistance of the load connected is of optimal value, like R_{opt} in figure 2.3a.

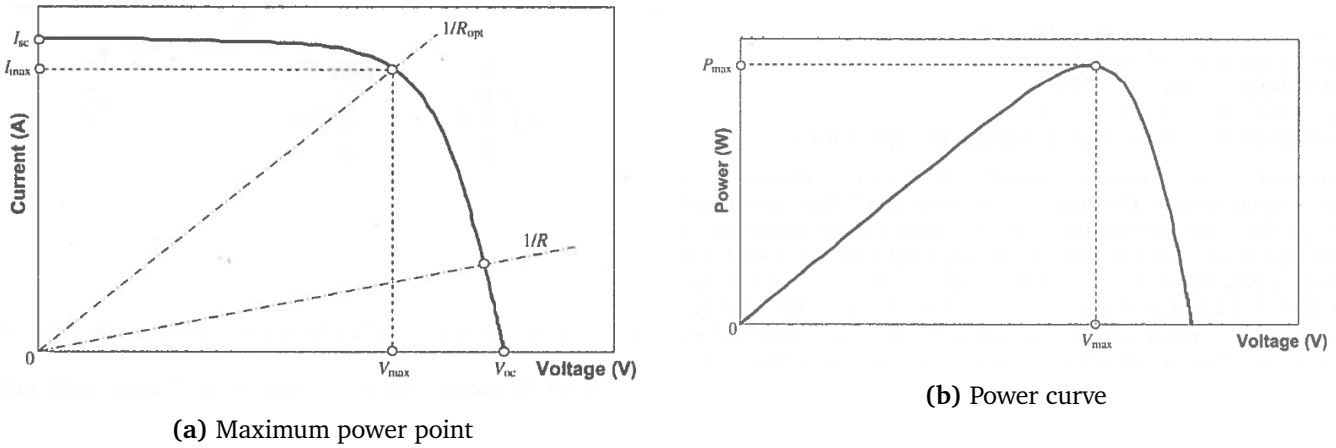


Figure 2.3: The I-V and power curve of a solar cell/module, modified figures from [2]

The efficiency of a solar cell is then given as the ratio of power the cell can produce to the incident power of the solar radiation. In terms of MPP voltage and current the efficiency η can be expressed as

$$\eta = \frac{P_{max}}{P_{in}} = \frac{V_{mp} \cdot I_{mp}}{P_{in}} \quad (2.13)$$

Many cells are also defined in terms of their fill factor (FF), which is a measure of losses in the cell. It is given as $FF = V_{mp}I_{mp}/V_{oc}I_{sc}$, yielding

$$\eta = \frac{FF \cdot V_{oc} \cdot I_{sc}}{P_{in}} \quad (2.14)$$

Maybe the most used term when classifying solar cells is watt peak W_p , or nominal power. It is defined as the maximum power produced under standard

testing conditions (STC), which again are specified as an irradiation of 1000 W/m^2 , an AM1.5 spectrum and a cell temperature of 25°C [12]. The theoretical limit (Shockley-Queisser) of single junction cells mentioned earlier has also been calculated for STC and was found to be 33.16 % for a band gap of 1.34 eV [14]. Some manufacturers also inform about performance of their cells under normal operating cell temperature (NOCT) conditions. The operating temperature varies and is usually given in module datasheets, but the NOCT conditions are defined as an irradiance of 800 W/m^2 , an ambient temperature of 20°C and a wind speed of 1 m/s [2].

2.3 The main technologies today

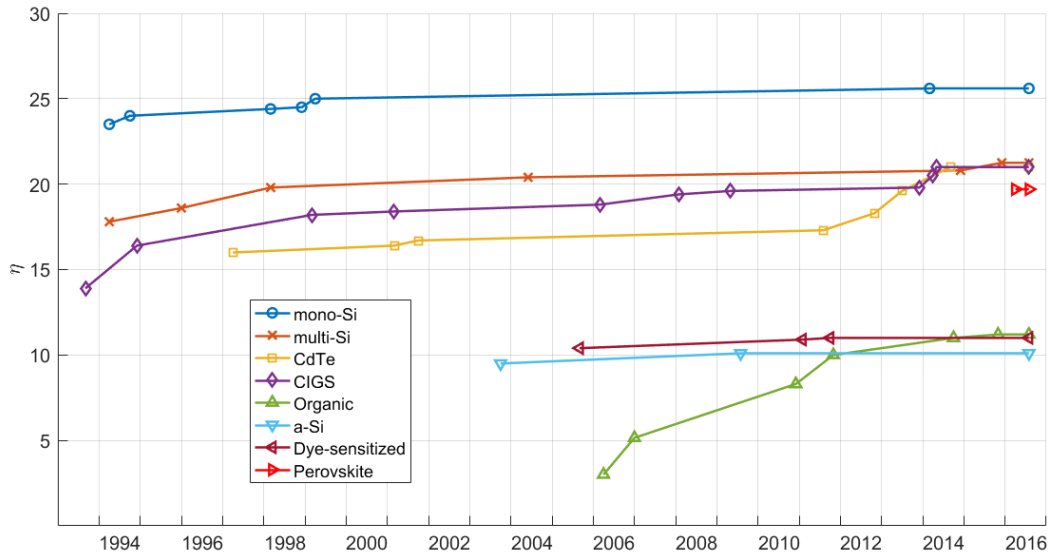
There are three types of solar cells that dominate the market today: Monocrystalline silicon (mono-Si), multicrystalline silicon (multi-Si) and various types of thin-film cells. In 2015 63.2 GW_p of solar cells were produced. About 69% or 43.9 GW_p of these were multi-Si cells, about 24% or 15.1 GW_p were mono-Si while the remaining 7% or 4.2 GW_p were thin-film cells [1].

As the names suggest, the crystalline structures are what separate mono-Si and multi-Si solar cells. The silicon in mono-Si cells has only one continuous crystal lattice with almost no defects or impurities, resulting in relatively high efficiencies [2]. But, because of advanced production processes the price of these cells is usually higher than other options on the market today. The fact that multi-Si cells consist of many mono-Si grains, and less complicated production processes, make these cells slightly less efficient but cheaper than mono-Si cells.

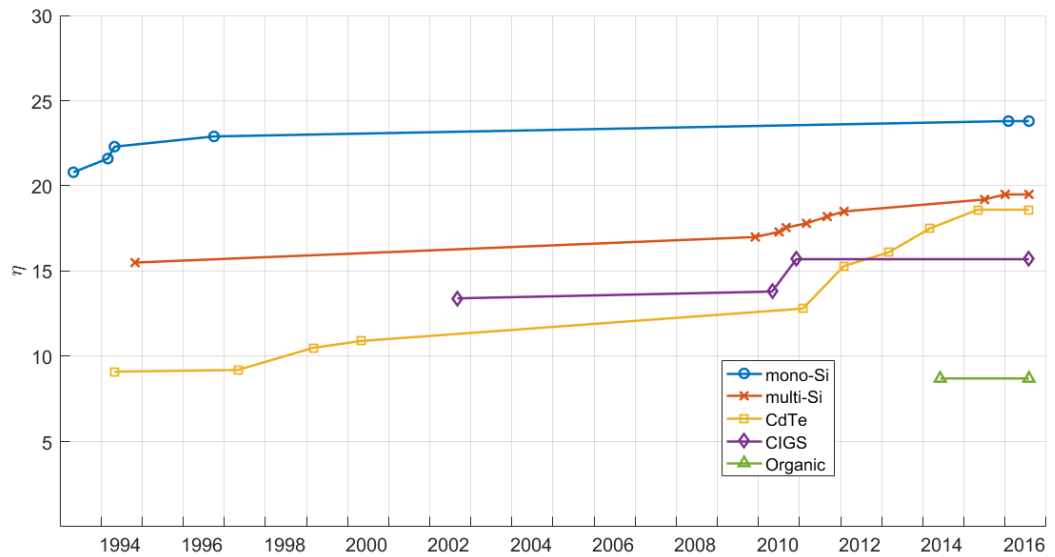
Thin-film cells are made up of extremely thin layers of photovoltaic material. The thickness of crystalline silicon wafers, or cells, usually goes up to $200 \mu\text{m}$, while thin-film cells go from a few nm to tens of μm . There are mainly three types of thin-film cells being produced on the market today: Cadmium telluride (CdTe), copper indium gallium selenide (CIGS) and amorphous silicon (a-Si). Out of the 4.2 GW_p thin-film cells produced in 2015, 2.5 GW_p were CdTe, 1.1 GW_p were CIGS and 0.6 GW_p were a-Si [1]. Emerging thin-film technologies include dye-sensitized cells and other organic cells. As thin-film cells are flexible, thin-film modules can be either fixed or flexible depending on the material used as the front and back of the module.

Lately, perovskite cells have also seen a tremendous development in efficiency, reaching just above 22% in early 2016. Although the fabrication process has given variable results and has seemed hard to master, things are beginning to look brighter. Low production costs, more stable results that have been

reproducible and efficiencies that may match crystalline silicon cells gives this type of solar cell a promising future [4]. The evolution of laboratory efficiencies for some types of solar cells and modules during the last two decades are shown in figure 2.4a and 2.4b. It should be mentioned that these figures represent record efficiencies done in laboratories and under standard test conditions (STC), and in most cases they are therefore higher than for typical commercial products. Commercial crystalline silicon modules have efficiencies between 14 and 21.5% while typical efficiencies of commercial thin-film modules range from 7% for a-Si to 16.3% for CdTe [3].



(a) Cells



(b) Modules

Figure 2.4: The evolution of PV efficiencies, data from [5]

2.3.1 Factors affecting efficiency and yield

The amount of irradiance as well as temperature have distinct effects on the performance of a solar cell, as shown in figure 2.5. The higher the irradiance the higher the yield, and the lower the temperature the higher the efficiency. It should be noted that higher levels of irradiance does not necessarily increase

the efficiency of a module. Depending on the technology, the efficiency below an irradiance of 1000 W/m^2 might be higher or lower than the efficiency measured at STC. Nevertheless, cold and sunny climates are ideal for PV systems. Materials/technologies respond to these changes differently though. Sensitivity to temperature is quantified using temperature coefficients, and maybe most interesting among them is the temperature coefficient of the module power. Specifically, this is the percentage of power lost with every $^{\circ}\text{C}$ relative to the nominal power.

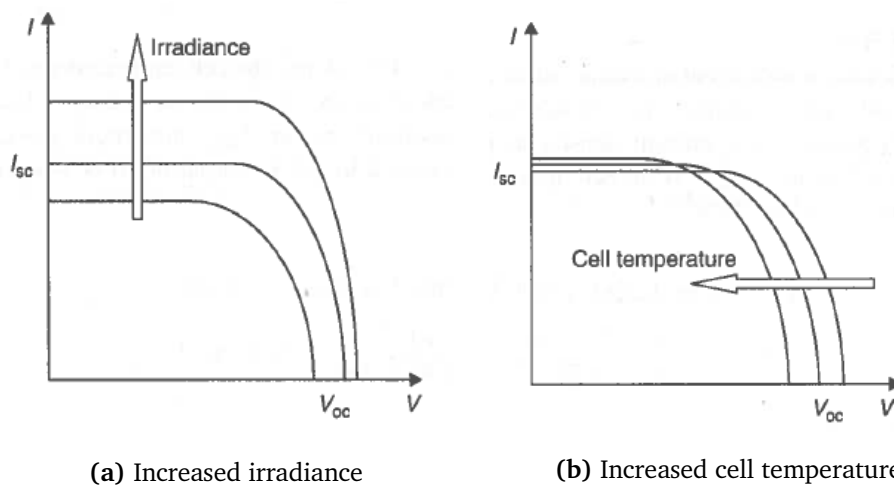


Figure 2.5: Effects of increasing irradiance and temperature on the I-V curve of a solar cell, from [2]

When comparing how technologies perform under varying spectra, the spectral response of the material is essential. The spectral response can be defined as the amount of current produced per watt of incoming irradiance as a function of the radiation wavelength. In figure 2.6a some typical c-Si and CIS/CIGS spectral responses are shown. Within each technology various products will have different responses, but as can be seen from figure 2.6b, at least differences between c-Si modules are not large compared to differences between technologies. As mentioned in section 2.1 the spectrum of incoming irradiance is changing with weather and the position of the Sun. Different technologies, some more than others, therefore tend to have a set of conditions in which they operate best. A low temperature coefficient would for example make a module an allrounder relatively speaking, not losing or gaining large amounts of power when operating in cold or hot climates. Large temperature coefficients would on the other hand be favourable if modules were to be cooled substantially under operation. Likewise, a broad spectral response ensures that a module has the ability to produce power under varying conditions such as

high air mass/low solar height and large amounts of diffuse radiation while also performing under bluer spectra when the Sun is at its highest. It has for example been reported that the performance of a-Si is very susceptible to changes in spectrum due to its narrow spectral response, as shown in figure 2.6c [76].

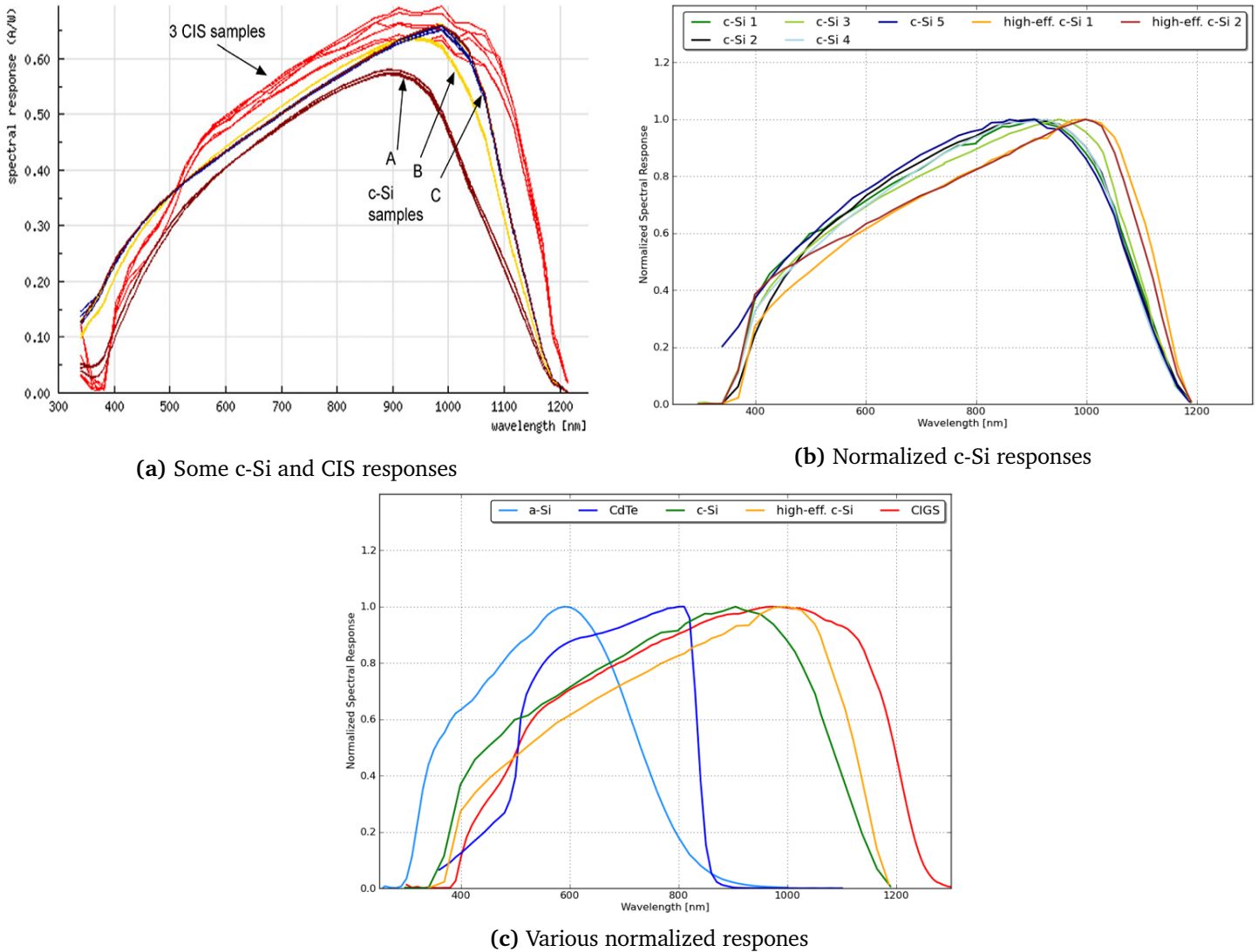


Figure 2.6: Spectral responses, from [48] and [15]

Mono/multi-Si and CIGS are the two technologies that will be looked at further in this thesis, as they represent most or all of the current grid-connected systems in Norway. CIGS modules generally have lower temperature coefficients than

c-Si modules. For example, [47] looked at silicon and CIGS modules with temperature coefficients of $-0.45\%/^{\circ}\text{C}$ and $-0.36\%/^{\circ}\text{C}$ respectively, but there are large differences between products as shown in chapter 5. On a general basis CIGS modules therefore perform better than under STC when operating at temperatures higher than 25°C , while crystalline Si modules perform better below this point.

As seen in figure 2.6a CIGS modules respond better to infrared radiation in particular, above about 1100 nm . Additionally, CIGS modules are not as severely affected by partial shading as c-Si modules, since the modules are not built up with the usual string structure.

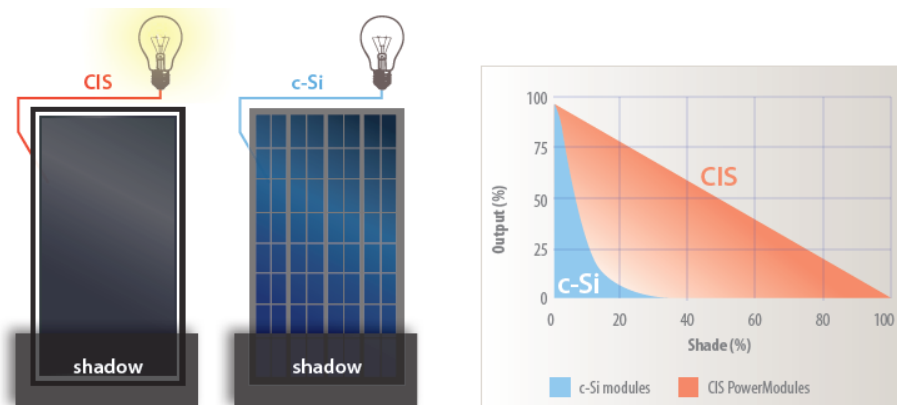


Figure 2.7: Illustration of shading effects on CIS modules, here by CIS manufacturer Solar Frontier [49]

As shown in figure 2.7 the decrease in power output from a CIS module is a linear function of the area being shaded. Lastly CIS/CIGS modules experience what is called a light-soaking effect where their efficiencies actually increase after being exposed to sunlight. This typically increases the efficiency of a CIS/CIGS module with 7-15% during operation compared to specified STC performance [50].

2.4 PV orientation, yield and time of production

The orientation of a PV system decides how much total energy will be available as well as when energy will be produced, both over a year and a day. Different orientations will be looked at in this thesis, including near horizontal, tilted south-facing and vertical modules. Because of the variation of solar height

during the year, various tilt angles will perform better during certain times of the year. Optimally tilted modules make use of the high irradiance during summer as well as the lower Sun in spring/fall. Steep/vertically mounted modules perform well during spring/fall and winter months but then again do not take advantage of the high summer Sun. This is illustrated in figure 2.8

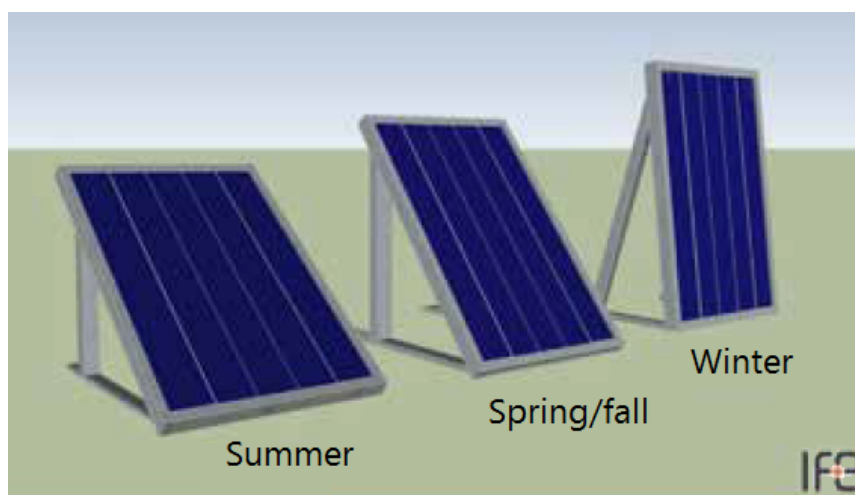


Figure 2.8: Optimal tilt angles for different parts of the year, modified figure from [51]

Modules tilted differently can also be said to make use of different parts of the incoming irradiance. Horizontal modules can make use of most of the sky diffuse irradiance, highly tilted modules will be susceptible to ground-reflected irradiance while modules tilted somewhere inbetween are efficient at using direct irradiance, especially during summer. Optimal tilt angles vary with latitude, and it has been empirically shown that the tilt angle which maximizes the annual energy yield of a PV array is given by [26]

$$\beta = \begin{cases} (0.764 \cdot L) + 2.14^\circ, & \text{if } L \leq 65^\circ \\ (0.224 \cdot L) + 33.65^\circ, & \text{otherwise} \end{cases} \quad (2.15)$$

where L is the latitude, and the azimuth is assumed to be close to true south. For locations in Norway, this means a tilt angle of around 48° : In Kristiansand and Tromsø the optimal tilt angles are 46.6° and 49.3° respectively. It should be noted that this equation does not take into account local weather conditions. For example, optimal tilt angles at locations with high amounts of diffuse irradiation may not be given by this relationship. Unless one has a roof with a tilt angle of 48° , free standing systems mounted this steep are rarely a viable option because of wind loads and self-shading.

More area-efficient solutions are therefore often chosen. Three of the systems looked at in chapter 5 are so-called east/west solutions, where the modules have

a low tilt angle and rows next to each other are facing in opposite directions. When placed east/west the system in theory should produce relatively well during morning, noon and afternoon but is maybe more importantly very area-efficient as nearly no distance is needed to avoid self-shading.

As a side note, different orientations of bifacial modules can also be mentioned for Norwegian conditions. They can convert light hitting both the front and back of the module and thereby increase yield substantially. As the gain in yield has been shown to be dependent on both surrounding ground albedo aswell as the amount of diffuse irradiation [53] [54], locations in Norway might be very suitable.

/3

Simulations in PVsyst

All the simulations performed by the author in this thesis, as well as some of those that have been done prior to installation of the systems looked at in chapter 5, have been done in the simulation program PVsyst. This chapter is therefore a short summary of how PVsyst simulates real conditions and what factors can be included in a simulation.

The first step in simulating a system in PVsyst is either importing meteorological data from measurements, other data sources or importing them from available models. GHI and ambient temperature are obligatory input data to perform a simulation, but additional factors like the direct/diffuse irradiance ratio, wind speed and array temperature can be imported. Regarding importing meteorological data from models, over a dozen options are compatible with PVsyst. Three free options included with PVsyst are looked at in this thesis: Meteonorm 7.1, PVGIS (classic and CM SAF) and NASA SSE.

PVGIS can be accessed online and consists of two databases: PVGIS classic and CM-SAF. The outputs used by PVsyst are average monthly GHI, ratio of direct/diffuse irradiation and ambient temperatures. The model calculates variables in a GIS program where layers of mainly geographical information as well as climate data are put on top of each other at a resolution of 1 km · 1 km. In the classic version irradiation data is gotten from 566 stations spread across Europe and is then interpolated between them. The only Norwegian station included is a station in Bergen. The newer Satellite Application Facility on Climate Modelling (CM SAF) version includes measurements from various

Meteosat satellites. The land coverage of these satellites has only extended to 58° north though, thus missing measurements from the entire Norwegian country [56] [55].

Metenorm is a pay to use software but hourly and monthly irradiation data is available through PVSyst. Monthly values are obtained from ground stations and is interpolated between the nearest three to obtain a complete map [58]. Current Norwegian Meteonorm stations with irradiation measurements available in PVSyst are Bergen, Bodø, Tromsø and Karasjok. Satellite data from Meteosat satellites is implemented aswell. NASA Surface Meteorology and Solar Energy programme (SSE) can lastly also be used directly in PVSyst. Averages are based on various databases with over 20 years of continous satellite data at a resolution of $1^\circ \cdot 1^\circ$. As this is quite coarse data, 1° latitude being equal to about 111 km, the accuracy of estimates will seldom be able to compete with models where ground stations are included [57]. Data for a given location from Meteonorm or NASA SSE can be imported through an interactive map in PVSyst while PVGIS has a website with its own interactive map.

If diffuse irradiation is not available through either imported measurements or data from models PVSyst calculates the diffuse fraction of the irradiation by the Liu and Jordan relation. Diffuse irradiation is here calculated as a function of the clearness index K_T , which again is given by the ratio of GHI to available extraterrestrial radiation [59] [60]. Furthermore, if only data on DHI exists, two transposition models can be chosen in PVSyst: The Perez model and the Hay model, both described briefly in section 2.1.1. Lastly, ground-reflected irradiance is calculated according to equation 2.4.

Far shadings can be included in a PVSyst simulation by drawing in objects blocking the horizon on a sun path diagram while near shadings are mainly taken into account through 3D-modelling of the PV system and its surroundings. To the author's knowledge none of the simulations in this thesis have gone through either of these steps. Most commercial modules and inverters are found in the PVSyst database including about 12500 modules and 4500 inverters. As mainly c-Si and CIGS modules are looked at in this thesis, it is also of interest to know how PVSyst simulates the difference between them. Temperature coefficients are given for each module in PVSyst and can also be changed manually. The light-soaking effect occuring in CIS/CIGS modules is included, with a standard 2% gain in yield. Low-light performance is taken into

Urban situation	0.14 - 0.22
Grass	0.15 - 0.25
Fresh Grass	0.26
Fresh snow	0.82
Wet snow	0.55 - 0.75
Dry asphalt	0.09 - 0.15
Wet asphalt	0.18
Concrete	0.25 - 0.35
Red tiles	0.33

Figure 3.1: Suggested albedo values from PVSyst

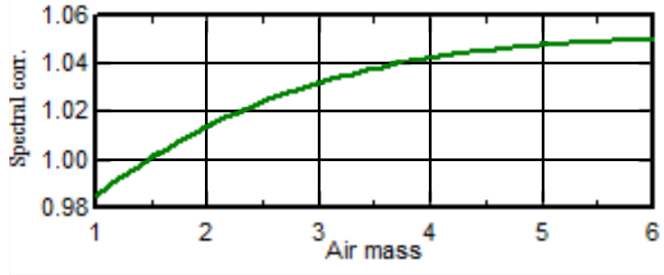


Figure 3.2: Spectral correction in efficiency as suggested by the Sandia Model for the mono-Si module SunPower SPR-225NE-WHT-D, modified figure from PVsyst

account, typically with a small decline in efficiency under low irradiance. Spectral corrections dependent on air mass alone can be included, but only for modules included in the Sandia Model [61]. Some mono/multi-Si modules are included here, but unfortunately no CIS/CIGS modules. The difference in spectral corrections between the two technologies can therefore currently not be simulated. As the spectral correction is only air mass dependent it is not taken into account whether the sky is clear or overcast. The correction might therefore tend to overestimate efficiency gains [62]. An example of the spectral correction suggested by the Sandia Model is shown in figure 3.2.

One can specify monthly albedo values in PVsyst, 0.2 being the default value. Some of the albedo values suggested by PVsyst for different surroundings/materials are shown in figure 3.1. Ambient temperatures and wind speeds either imported or generated from models within PVsyst affect simulation results through a thermal model expressed by the two equations

$$U \cdot (T_{cell} - T_{amb}) = \omega \cdot G_t \cdot (1 - \eta) \quad (3.1)$$

$$U = U_c + (U_v \cdot v) \quad (3.2)$$

where U is the thermal loss factor split into a constant term U_c and a wind speed coefficient U_v , v is the wind speed, T_{cell} and T_{amb} are the cell and ambient temperatures and ω is the absorption coefficient of incoming irradiation. By default PVsyst sets ω to 0.9. Both U_c and U_v can be chosen for each simulation manually, and if U_v is set to zero the wind-dependent factor is incorporated into the constant factor assuming a wind speed of 1.5 m/s [63]. The incidence angle modifier (IAM) is also definable in PVsyst. It is a factor that is meant to represent losses occurring as a result of light being reflected away when the AOI is suboptimal/nonzero. PVsyst models this using the American Society of Heating, Refrigerating and Air-Conditioning Engineers (ASHRAE) parametrization

$$F_{IAM} = 1 - (b_o \cdot (\frac{1}{\cos(\theta)} - 1)) \quad (3.3)$$

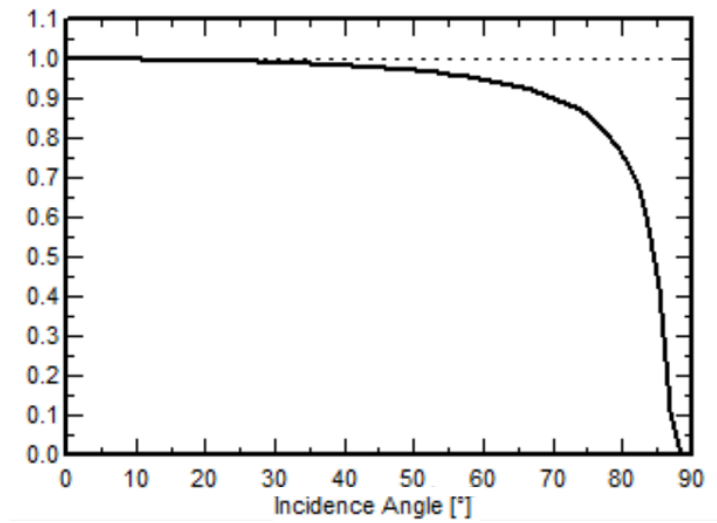


Figure 3.3: The default ASHRAE incidence angle modifier in PVsyst

which is only dependant on b_0 . This factor again depends on the type of module, types of anti-reflective coating and so on, but PVsyst sets it to 0.05 by default [64]. It can be changed manually or points on the curve in figure 3.3 can be specified in order to obtain special cases of IAMs. Lastly, soiling losses can be defined either as annual or monthly losses in yield and the light induced degradation (LID) which occurs when c-Si cells are exposed to light can also be included in simulations as a simple loss in yield [77].

/4

Norwegian conditions for PV

4.1 Available data and the effect of the Norwegian climate on PV performance

To precisely predict the yield of a PV system, relevant irradiation data needs to be available either by models or measurements. A measuring device at a potential project location is always preferable, but because of cost and time use this is rarely a viable option. Other tools or options then need to be considered, but one is then generally left with two choices: An average of data from the closest measurements available could be taken, or tools that estimate average irradiation could be used. There are mainly two problems that arise when these tools are used for high latitude locations like Norway though: Firstly satellite data is often coarse or does not exist for high latitudes and secondly Norwegian ground stations included in the available tools are few, like mentioned in chapter 3. There are more stations which measure solar irradiation to be found in Norway, and to get an idea of what was available as well as what actual average measurements were at different locations, some irradiation data has been collected. Additionally, as a part of this thesis was to compare simulated/expected yields with measured data, it was important to get a general understanding of how the irradiation models that make up the foundation of the simulations compare to actual measurements.

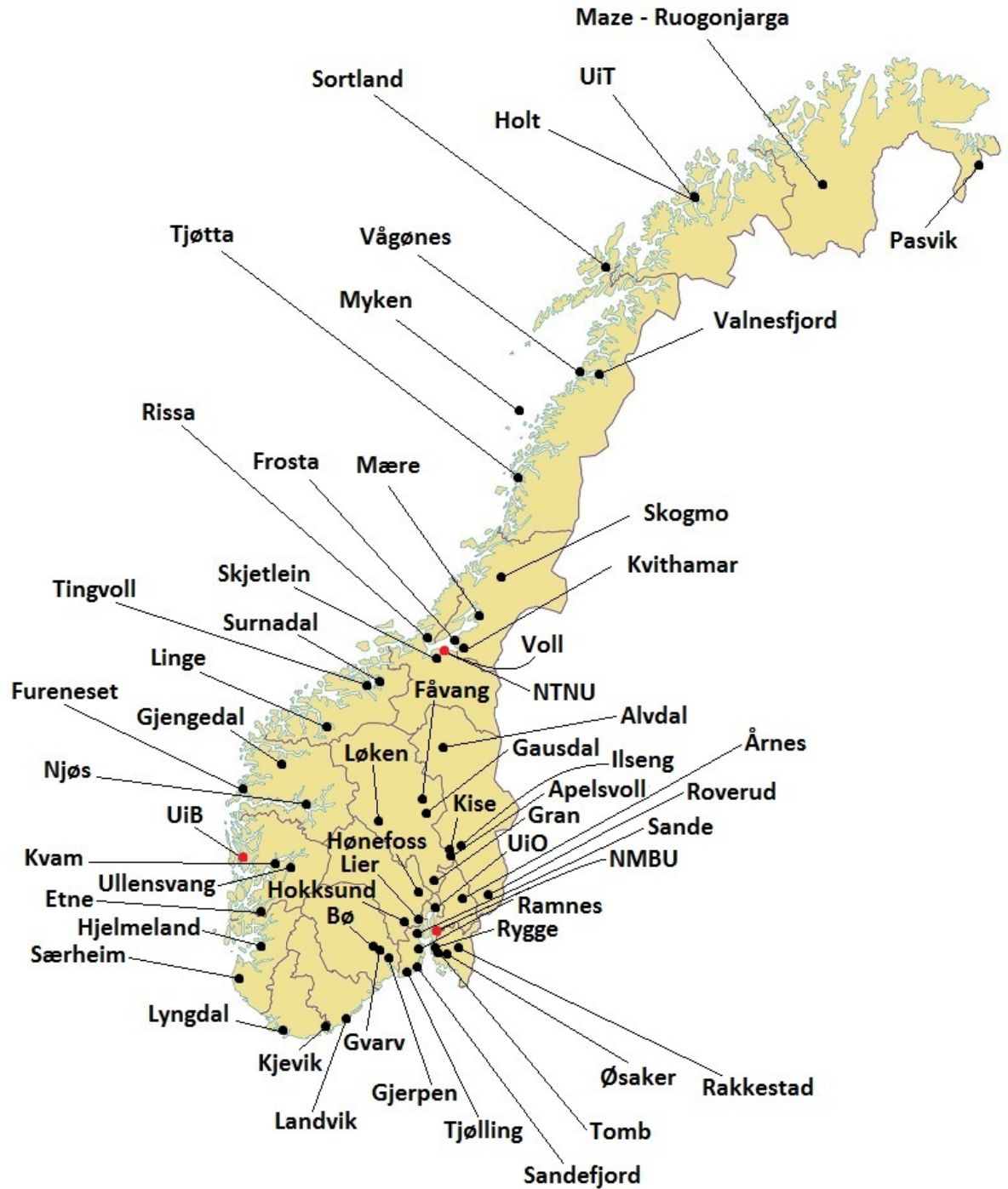


Figure 4.1: Locations where irradiance data was available, red dots indicating data including both global as well as direct and/or diffuse irradiance (base map by Kartverket)

The locations where irradiation data was gathered from are shown in figure 4.1, while actual values are listed in table B.1. The data was mainly retrieved from the meteorological service for agriculture in Norway (Landbruksmeteorologisk Tjeneste, LMT), the Norwegian Meteorological Institute (MET) and the universities of Trondheim, Bergen and Ås. Although not a complete list of what irradiation data is available in Norway, it includes 57 locations with the average period of data being 17 years. Like expressed in [22], these measurements should be cross-checked with existing tools to get an idea of what tools work and do not work for Norwegian locations, as well as to lead to possible improvements in the models. To see if there were large differences between some of the existing tools, Meteonorm 7.1, PVGIS and NASA SSE were tested against the collected data. This was done by computing root-mean-square error (RMSE) according to

$$\text{RMSE} = \sqrt{\frac{\sum_{n=1}^N (\hat{y}_n - y_n)^2}{N}} \quad (4.1)$$

where \hat{y}_n is the measured annual irradiation, y_n is the predicted annual irradiation and N is the number of locations. Meteonorm and PVGIS ended up with pretty equal errors at 71.8 kWh/m²/year and 69.6 kWh/m²/year respectively while the SSE had an error of 86.1 kWh/m²/year. SSE ending up with such an error is maybe not surprising as it is based on satellite data alone and has a resolution of 1° x 1°. It should be mentioned that some of the measured datasets stretch as far back as 1986, and after contacting LMT it was not possible to get an overview of equipment used throughout the years as well as the quality of the data. At some locations annual irradiation varies significantly just within a few kilometers. Tromsø is such a case where Holt, UiT and the Meteonorm station gave values of 656, 801 and 735 kWh/m²/year respectively. A quick look at what the cause of this may be was taken but no satisfactory answer was gotten. As a side note it can be mentioned that short bursts of irradiance over 1300 W/m² were observed in the UiT dataset. The maximum value found was 1334 W/m² on the 15 June 2010, possibly adding to the cases of overirradiance caused by forward scattering from cloud cover as described in [39].

It was originally of interest to gather some data on the ratio of direct/diffuse irradiation for some locations as well. Three universities had available data on this: The universities of Ås (NMBU), Bergen (UiB) and Trondheim (NTNU). As only DNI was measured at NTNU, DHI was obtained by using equation 2.6. Plots of the averages of global/diffuse irradiation for these three locations are shown and further discussed in chapter 6, showing that 58.5%, 54.2% and 45.8% of the average annual irradiation is diffuse irradiation in Trondheim, Bergen and Ås respectively.

Temperatures in Norway increase the yield of PV systems. Although the lowest

temperatures occur during winter months when there is little irradiation, see for example figure C.1c and 6.1c, some months like march can end up giving relatively high yields. Snow cover can increase and decrease PV yield. Modules placed nearly horizontally will be covered by snow for some percentage of winter months. The steeper (larger tilt angle) the modules are mounted, the less of a problem this will be. Vertically mounted modules can avoid this problem almost completely while fully taking advantage, under the assumption that ground-reflected irradiation varies according to equation 2.4, of the benefit of the snow; Increased ground albedo. The only way increase ground-reflected radiation even more would be installing at tilt angles above 90° , but this is seldom/never a viable option. One source on the average monthly albedo in Norway was found at NMBU and are shown in figure 4.2.

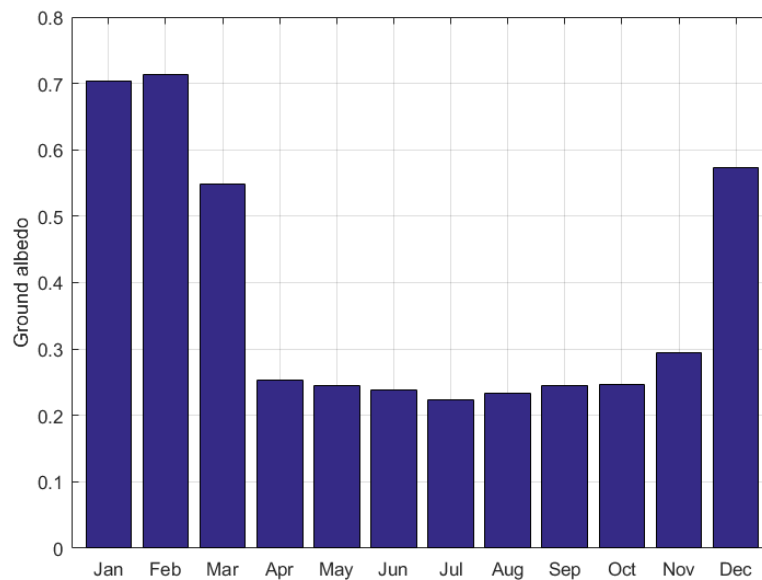


Figure 4.2: Average monthly values of ground albedo at Fagklim, Ås 2009 - 2015 [40]

The measuring setup here consists of a pyranometer flipped upside down measuring the ground-reflected irradiation [41]. When compared to the incoming global irradiation, the albedo can be found as the ratio of the two. Not surprisingly january, february, march and december are the months with the most frequent snow cover and thereby also the highest ground albedo values. PVsyst takes an albedo of 0.2 as a standard value, and the rest of the months seem to fit this rather closely. Keeping irradiation and temperatures in mind, february and march can thus be months of higher relative yield. Depending on the application and mounting of the system, these months are also periods of possibly large soiling (snow cover) losses. Lastly, Norway lies at a high latitude and the air mass is generally high. Because of Rayleigh scattering this affects

both the amount of diffuse irradiation as well as the spectrum of the direct irradiation. For example, [67] confirmed a general red richness in the spectrum at Kjeller and Grimstad.

4.2 Literature review of PV performance in Norway

A brief search has been made to see what existing literature says about the performance of PV in Norway. In [65] the details of an established measuring station at Grimstad is presented and key data on three technologies under operation is given. Mono-Si, multi-Si and s-Si were tested and mono-Si turned out to perform best while a-Si performed worst. Although a remark is made that measurements are by no means precise the authors conclude with PV being a viable option in Norway. Another test station located at the University of Agder is presented in [66]. This station included mono-Si, multi-Si, CIS and a-Si modules. Some measurements of temperature from the back of the modules as well as I-V curves and power curves for some days are included. In [68] the performance of north-facing multi-Si modules is studied and concludes with a significant yield. A two-axis tracking system located in Narvik is described in [69], which concludes with a significant increase in yield compared to fixed-tilt systems, especially during summer months. [70] describes field stations in Norway and Kenya testing the same types of Elkem Solar multi-Si modules. Generally speaking the found literature can be said to conclude with PV being a viable option Norway.

/5

System performance studies

Monthly and hourly yield has been gathered from five different PV systems in Norway and is presented together with expected yield in this chapter. The yield data has been made available to the author via the sites of SMA Sunny Portal, Delta Energy Systems and BuildingOS. Simulated/expected values of yield were downloaded from the same sites or gotten from contacting system owners/suppliers. What the different system simulations were based on, especially regarding irradiation data has also been looked at. When available these modeled values were then compared to the nearest irradiation data found. Lastly, a quick look at what might have caused shading and soiling (snow cover) losses at each system is taken.

5.1 Haakonsvern ZEB, Bergen

This PV system located at the naval base Haakonsvern roughly 8 km from Bergen was operational by november 2015. It is found on what aimed to be one of the most energy effective buildings in Norway, with an estimated energy use of 16 kWh/m²/year in addition to the consumed energy from a seawater heat pump and the locally produced solar power [29]. These estimates assumed that 26 kWh/m²/year, or roughly 53 MWh/year when considering the 2010 m²

of space in use in the building, would be produced by the PV system.

Table 5.1: The system at Haakonservern

Modules	254 x BenQ SunForte PM096Boo
System power/inverters	84.6 kWp / 4 x SMA STP20000TL-30
Orientation	$\alpha_a = \pm 90^\circ$ (east/west), $\beta = 10^\circ$
Price	Roughly 2 million NOK, 23.6 NOK/Wp

To achieve this, the PV system was sized to consist of 254 modules with 333 Wp each, making the total nominal power of the system about 85 kWp. Being connected to the grid, the system can always feed electricity to neighboring buildings if there is a need for it, making batteries and control systems unnecessary. Specifications of the system and modules are listed in table 5.1 and 5.2.



Figure 5.1: Part of the system at Haakonservern shortly after it's installation, photos: Arild Lunde

Prior to the installation simulations were done and concluded with an average yield of 56.1 MWh/year. These monthly estimates can be seen in figure 5.2b labeled as the original estimate. Simulations were done in PVsyst and assumed a 86.9 kWp system mounted horizontally. Irradiation data generated by Meteonorm 6.1 was used and the diffuse irradiation gotten using the Erbs decomposition model, which in newer versions of PVsyst is replaced with the Liu and Jordan model. The actual yield of 55.1 MWh, measured from december 2015 to november 2016, is roughly the same as the estimate, but monthly deviations are observed. When comparing the yield to available data on measured

GHI for Flesland, about 5.5 km from Haakonssvern, the two follow each other closely except for may and june, as shown in figure 5.2. The main cause of this was found to be a malfunctioning circuit breaker, resulting in an estimated yield loss of 3-4 MWh. When adding 1.75 MWh to both of these monthly yields, as shown with the dashed red line in figure 5.2b, they fit the whole picture better. The corrected annual yield then ends up at 58.6 MWh, 4.5% higher than what was estimated. Arguing from the close relationship between the irradiation and yield curves, most of this can be said to be a result of actual irradiation having been 10.8% higher than estimated. Using the corrected yield, the specific

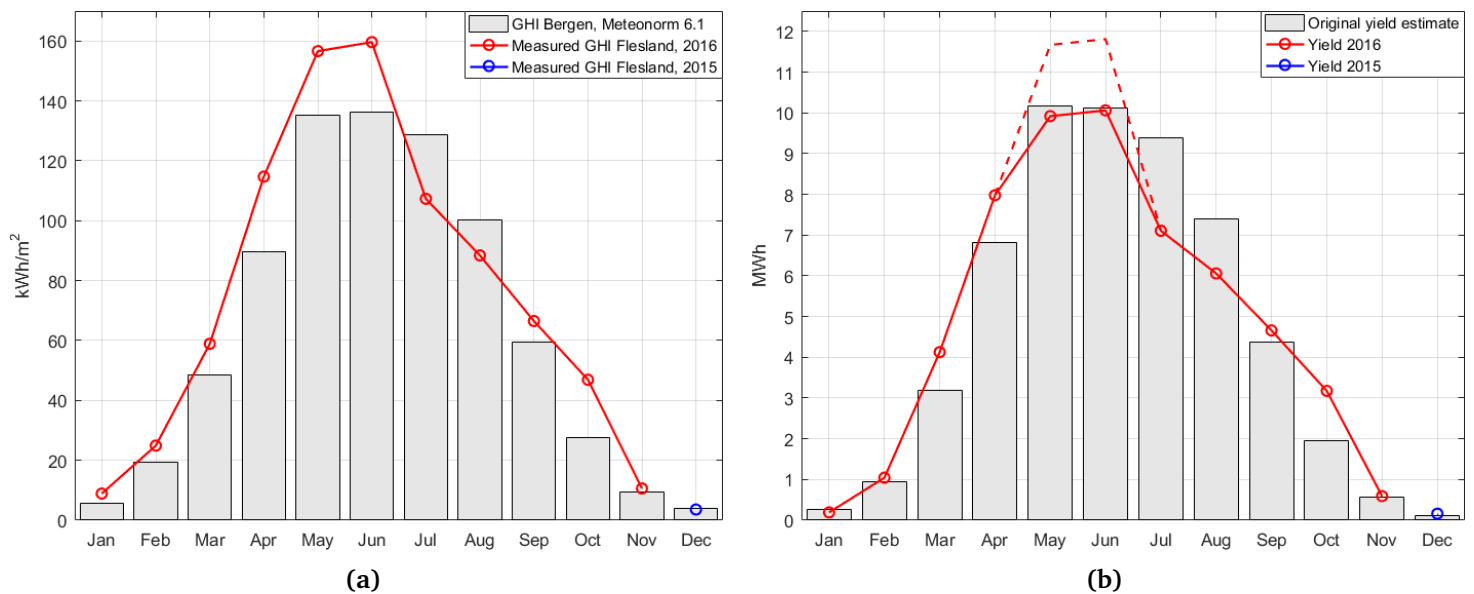


Figure 5.2: Expected and measured irradiation and yield, GHI measurements from eklima.no and yield data from sunnyportal.com

annual yield of the system ends up at 692.7 kWh/kWp, while actually logged values amount to 651.3 kWh/kWp. The estimated annual specific yield was 645 kWh/kWp. The relatively low irradiation in July was mainly result of a rainfull and cloudy month. Although Bergen is known to many for its high amounts of rainfall, 2016 turned out to be a record breaking

Table 5.2: Technical data on the SunForte PM096Boo module, from [28]

Technology	mono-Si
Efficiency, η	20.4%
Nominal power, P_N	333 W
STC MPP current/voltage	6.09 A/54.7 V
Temp. coefficient of P_N	-0.33%/°C
Module area	1.63 m ²

year: There had not been more precipitation during the month of July since 1970 [42]. Hourly precipitation for 2016 is shown in figure 5.3, illustrating this. Worth noting is also that the period from March to June as well as October had little precipitation and high amounts of irradiation compared to what was estimated.

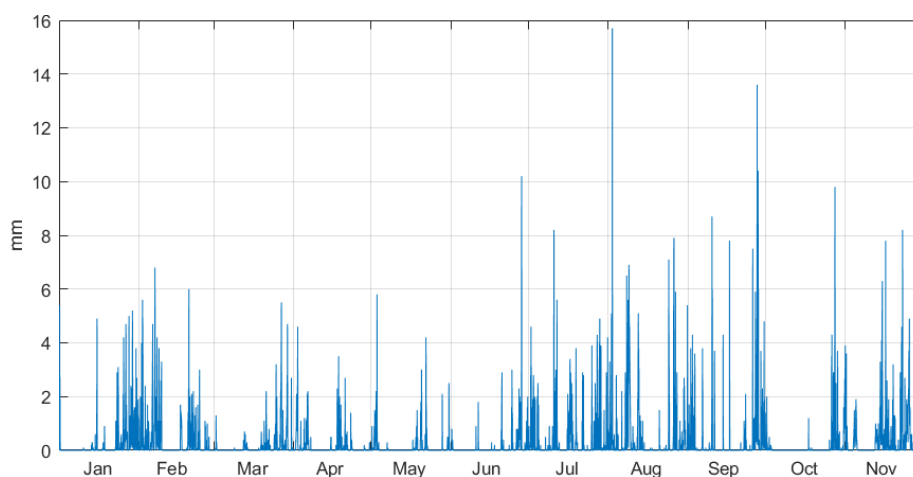


Figure 5.3: 2016 hourly precipitation at Flesland, data from eklima.no

Contacting project manager Arild Lunde at Forsvarsbygg revealed that a nearby hill was causing shading losses during afternoon hours of some winter months. To quantify these losses a simulation has been performed using irradiation and temperature data for 2016 from Flesland. These results are then compared to average hourly specific yields for each month. Shading losses have been neglected here and soiling losses were set to 2% of annual yield. Furthermore the simulation was based on a slightly larger system than the actual one, with nominal power of 84.8 kWp. Thus, the simulated yield could be thought of as a rough maximum of what the actual system should have produced. Comparison reveals two things: Firstly, the effect of the malfunctioning circuit breaker is mainly shown as reduced yield around midday in May and June, and secondly reduced yield in January, February, November and December are shown for afternoon hours. Based on the difference between the measured and simulated power the shading caused by the nearby hill has resulted in a decrease in yield of about 380 kWh, 792 kWh, 116 kWh and 58 kWh in January, February, November and December respectively. Totally this amounts to 1.35 MWh.

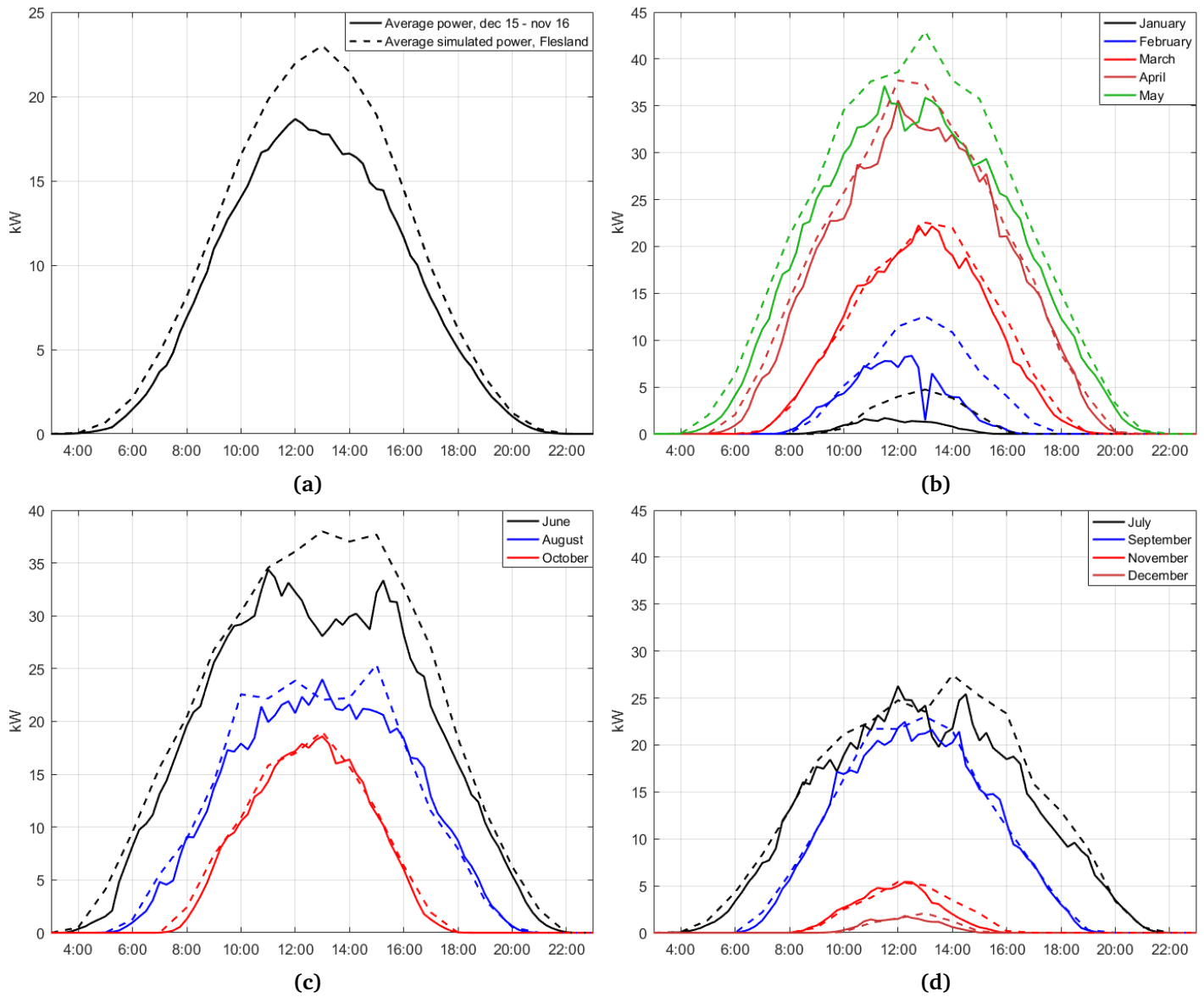


Figure 5.4: Average hourly power in comparison to a simulation based on 2016 irradiation and temperature data from Flemland (eklima.no)

5.2 Solsmaragden, Drammen

Because of its green power producing facades, this building in Drammen has gotten the name Solsmaragden, translating to Solar Emerald or equivalent names. It features a 183 kWp PV system which includes a roof mounted

PV subsystem in addition to the multiple power producing facades. Belgian supplier ISSOL delivered the BIPV solution, where mono-Si modules of different shapes are placed between two 4 mm safety glass plates and then laminated together [31]. This way already existing glass mounting brackets could be used to attach the "modules" while assuring safety: Glass plates are not able to fall down even if damaged. Solsmaragden was the first project in the world where this solution was made full use of [33].

A green print on the front glass plates also allowed the project to spread a signal of environmental consciousness. It should be noted that this print is estimated by the supplier to have lowered the output of the facades by 17% in comparison to non-printed PV glass [32]. The entire PV system including the different facades and

the roof, was installed by september 2015, but yield data available at the project's Sunny Portal site exists only from january 2016 and onwards. Technical data on the system and modules is shown in table 5.3, 5.4 and 5.5. Note

Table 5.3: Technical data on the IBC MonoSol 280 ZX module, from [30]

Technology	mono-Si
Efficiency, η	17.4%
Nominal power, P_N	280 W
STC MPP current/voltage	8.5 A/32.9 V
Temp. coefficient of P_N	-0.42%/°C
Module area	1.61 m ²

that data on only one of the ISSOL module shapes was found, and as the sizes of the modules installed on the facades varies, these specifications will not represent every single BIPV module in this system. Original estimates predicted a annual yield of 105.5 MWh, but seem to have been based on the assumption that the installed power in some of the facades was greater than what was actually installed. This has been corrected for by using estimated specific yields calculated by supplier ISSOL to then calculate correct monthly yields for each facade.

What irradiation data both the estimates for the facades aswell as the roof system is based on has not been found, and comparing irradiation data is rather useless here. It was mentioned by Steinar Nilsen of supplier FUSen that the roof yield had been simulated using IBC's solarcalculator, where NASA irradiation data might be used as a foundation. NASA SSE data for Oslo is therefore included in figure 5.6a. How supplier ISSOL has simulated yield is unfortunately not known to the author. While the estimates found on Sunny Portal summed up to a total annual yield of 105.6 MWh, the corrected one equals 101.8 MWh. By november the system had produced 94.6 MWh, 6.7 % lower than estimates for the same period. Measured GHI from Lier, the nearest measuring station that was found at about 6.6 km away from Solsmaragden, is also plotted in figure 5.6a. Comparing figures 5.6a and 5.6b shows that

irradiation and yield follow the roughly the same pattern, indicating that the measurements from Lier are representative of conditions in Drammen. From figure 5.6c it is clear that the higher yield in may - july was caused by the subsystem on the roof having much higher yields than expected.



Figure 5.5: The curved western facade and roof of Solsmaragden, photos from [31]

To look at how the different parts of the system were performing each month the specific yields are shown in figure 5.8a. The southwestern facade performs relatively well over the whole period and has more than double that of the other's specific yields in february. As seen in figure 5.6a, february and september were relatively sunny months, resulting in high yields from the southwestern facade especially. The western- and southern facades also have responded noticeable here. In figure 5.8c expected specific yields are compared to measured ones, showing that the southern facades are the biggest dissappointments by far, followed by the eastern facades. Losses from the green print are also shown here, and they amount to 9.06 MWh, or about half of what the entire northwestern facade has produced so far. The main reason for the low performance of the southern facades is likely to be shading caused the building itself; Once the Sun moves westwards of true south the facade facing southwest will cause shading on the facades facing south to a varying degree depending on solar height etc. An overview of the building and the different facades is shown in figure 5.7.

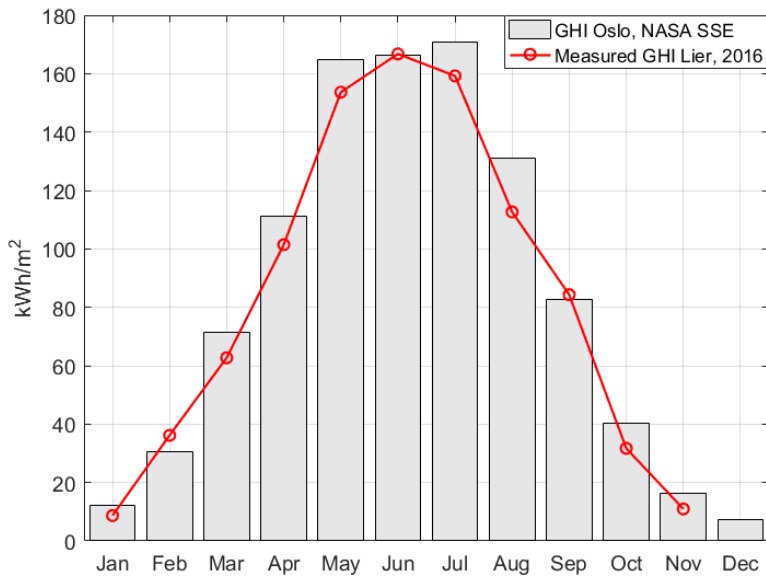
Table 5.4: Technical data on the ISSOL Cent 220 Model 160, from ISSOL presentation of Solsmaragden

Technology	mono-Si
Efficiency, η	$(15.8 \pm 0.1)\%$
Nominal power, P_N	160 W
STC MPP current/voltage	7.41 A/21.42 V
Temp. coefficient of P_N	$-0.391\%/^{\circ}\text{C}$
Module area	1.47 m^2

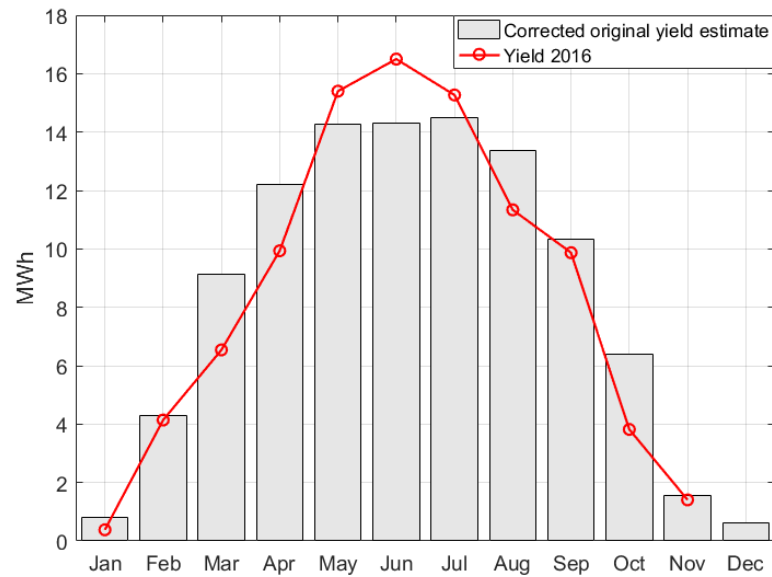
Table 5.5: The system at Solsmaragden

	Roof	Facades
Modules	242 x IBC MonoSol 280 ZX	1242 m ² of ISSOL Cenit 220 in different shapes
Nominal power	67.8 kWp	115.2 kWp divided as follows: Eastern: 3.6 kWp, southern: 19.9 kWp, western curve: 12 kWp, southwestern: 27 kWp and northwestern: 52.7 kWp
Inverters	SMA STP17000TL-10 2 x SMA STP25000TL-30	SMA SB3000TL-21 SMA STP5000TL-20 2 x SMA STP6000TL-20 2 x SMA STP10000TL-20 2 x SMA STP12000TL-20 SMA STP15000TL-10 SMA STP20000TL-30
Orientation	$\alpha_a = 115^\circ/295^\circ$ (southeast/northwest), $\beta = 10^\circ$	$\alpha_a = 90^\circ, 180^\circ, 205^\circ, 205^\circ - 295^\circ$ and $295^\circ, \beta = 90^\circ$

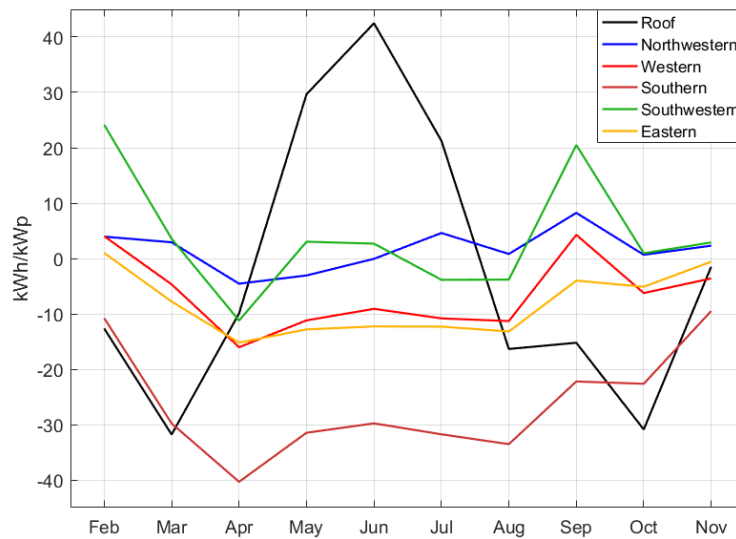
This effect is made clear by looking at the average hourly yields plotted in figure 5.8b, where the yield of the southern facades has a distinct peak at 12:00 and then decreases rapidly, whereas the southwestern facade, not being subject to shadowing of this degree, has a far better average yield between 12:00 and 20:00. Like shown in figure 5.8c, the southern facade actually performs the worst out of all the different parts of the system because of it. It should also be noted that the facade with the highest installed nominal power by far, the northwestern facade with 52.69 kWp, only had a specific yield of 321.8 kWh/kWp during the period february - november, making it discussable if installing such an amount here, in addition to on the southern facade, was the right choice. On the eastern side of Solsmaragden lies a building housing a large transformer as shown in figure 5.10. Consequently both the eastern and southern facades are experiencing some degree of shading because of it. Pointing exactly at what the effects of this have been is difficult though. A guess is that the output from both facades has been constantly lowered: Judging from pictures the building is only shading the lower parts of the facades. More precise statements could be made in the future, as the building is planned to be demolished.



(a) Monthly irradiation, measurements from lmt.bioforsk.no



(b) Total monthly yield measurements and estimates



(c) Differences between measured and estimated specific yields for the different parts of the system, positive values indicating better performance than expected

Figure 5.6: Some comparisons of monthly irradiation, yield and specific yields

Like seen in figure 5.8d, the hourly yield of the total system is higher in the period from 15:00 to about 21:00 in comparison to the period between 8:00 and 10:00. Figure 5.8b shows that this is due to the amount of power installed in the three facades facing west, southwest and northwest. Regarding snow on the nearly horizontal roof mounted modules a quick look at what the yield

data showed was taken. Like shown in figure 5.9, the period 1/3 - 10/3 includes almost no yield from the modules on the roof. Yields from the facades, especially the ones facing south, are also low in this period, but not as nonexistent as the ones from the roof. This may indicate a slightly lower irradiation and a snow cover on the roof. From the data available this was the only period found possibly indicating snow cover losses.

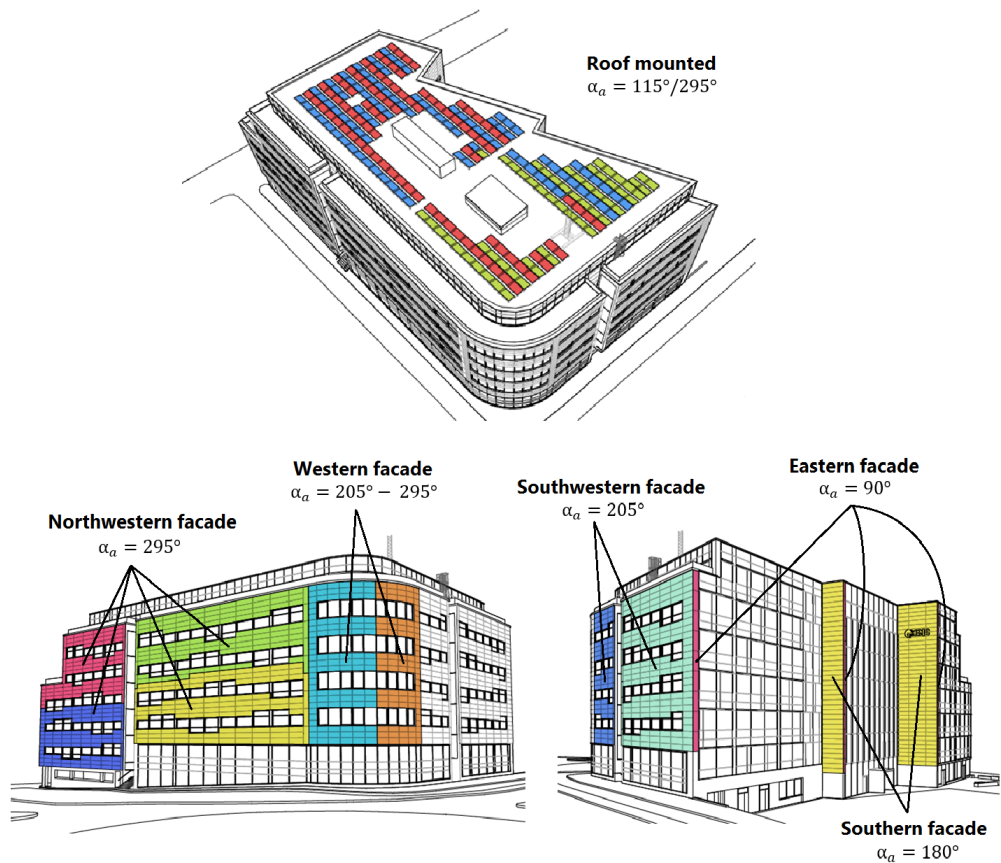
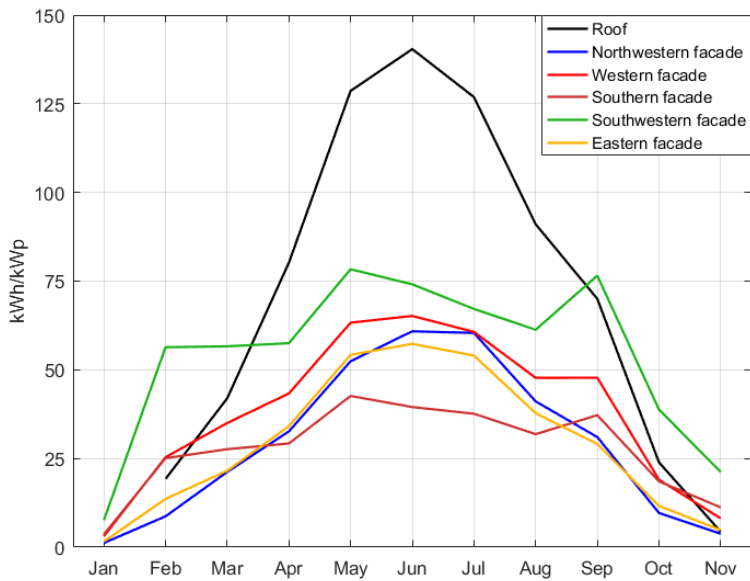
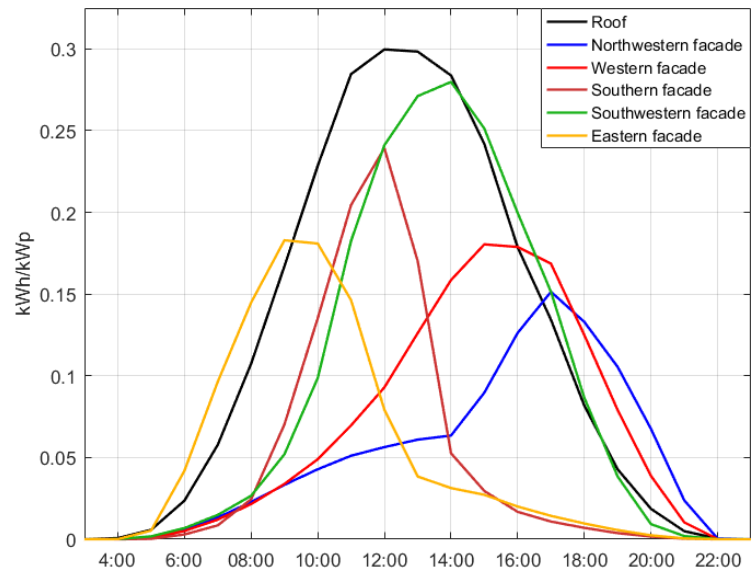


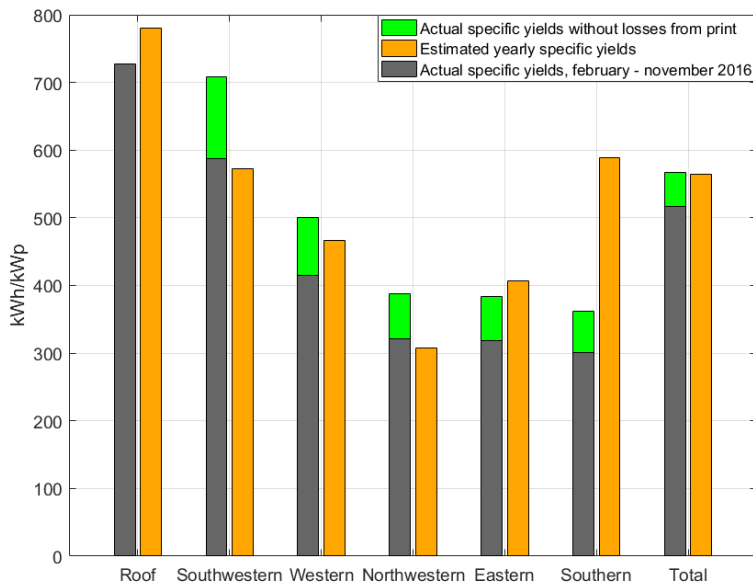
Figure 5.7: An overview of Solsmaragden, colors indicating different inverters
Original sketches gotten from Christine Wangnes, Union Eiendom



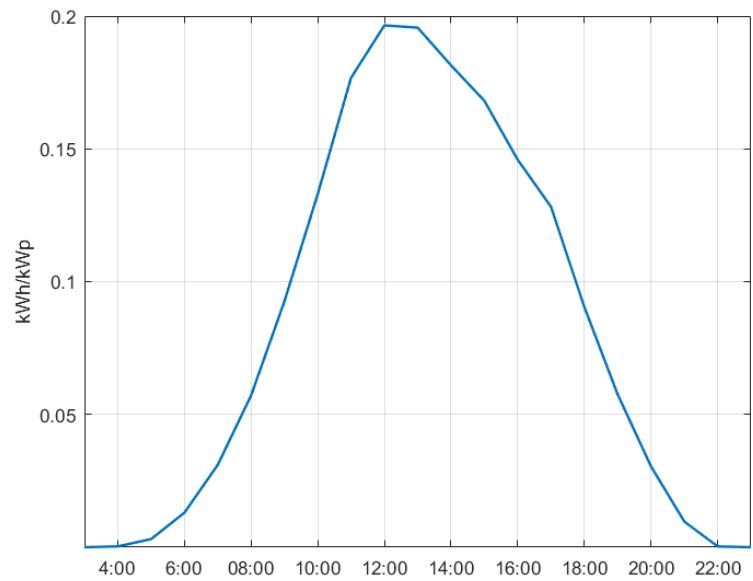
(a) Monthly specific yields of the different parts of the PV system at Solsmaragden, note that data for two weeks of april are missing



(b) Average hourly specific yields for the different parts of the Solsmaragden PV system



(c) Comparison of the specific yields for the period



(d) Average hourly yield of the total system, february - november

Figure 5.8: Monthly and average hourly specific yields of the different parts of the Solsmaragden system



Figure 5.10: The eastern side of Solsmaragden showing the transformer close by, photos gotten from Christine Wangsnes, Union Eiendom and FUSen.no

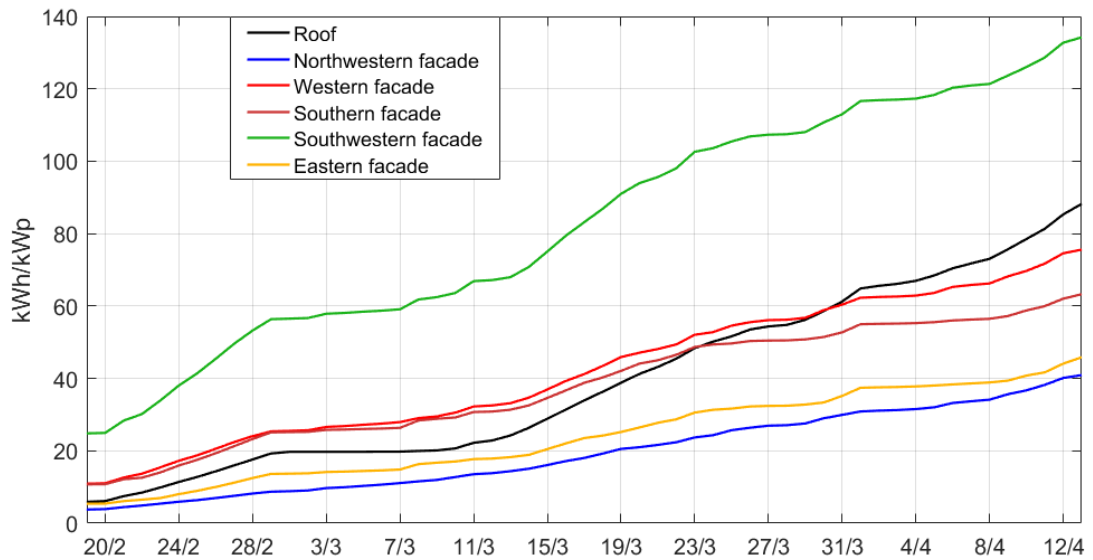


Figure 5.9: Cumulative specific yield of the different parts of the Solsmaragden system, indicating snow on the roof in the period around 1/3 - 10/3

5.3 Grøndalen Gård, Auli

At Grøndalen Farm, about 37 km northeast of Oslo, the first CIS/CIGS PV system in Norway was up and running by december 2015 [43]. The nominal power of the system is 70 kWp and it is mounted at two tilt angles facing southeast. The

smaller group of modules in figure 5.11 separated from the rest is installed at a tilt angle $\beta = 30^\circ$ and amount to 8.25 kWp, while the remaining 375 modules have a tilt angle of $\beta = 35^\circ$. In figure 5.13 monthly values of measured and predicted irradiance and yield is plotted. The measured irradiance in figure 5.13a was supplied by Karl Andreassen, COO of Green Energy A/S. The data has been measured using a reference silicon cell mounted with the same orientation as the main part of PV system ($\beta = 35^\circ$). From december 2015 - november 2016 the inverters had logged a production of 52.7 MWh, 19.5% lower than the predicted 65.5 MWh. Estimated specific yield was thus 935.2 kWh/kWp while the actual value ended up at 751.7 kWh/kWp.

The estimates in figure 5.13b were done in PVsyst by module supplier Solar Frontier and were based on the irradiation data from PVGIS shown in figure 5.13a. Simulated system size was 70 kWp, and all modules were set to tilt angles of $\beta = 35^\circ$ and an azimuth angle of $\alpha = 150^\circ$. The Erbs decomposition model was again used to model the diffuse fraction of irradiation and the Perez model was used to transpose it. Thermal loss factors U_c and U_v have been set to 26.7 and zero W/m^2K respectively. Lastly the CIS/CIGS light-soaking effect was modeled to give a 2% gain in yield, the b_o parameter included in the ASHRAE parametrization of AOI losses has been set to 0.04 and the monthly albedo values shown in figure 5.12 were used.

The measured 2016 yield was 19.5% lower than expected yield, whilst the irradiation was slightly higher than expected, so there have clearly been large losses present. No battery is installed at Grøndalen and excess power is sold to the local grid operator, Hafslund.



Figure 5.11: The PV system at Grøndalen Gård, photo: Karl Andreassen, Green Energy A/S

Table 5.6: The system at Grøndalen Gård

Modules	425 x Solar Frontier 165-S
System power/inverters	70.1 kWp / 13 x Delta RPI H5A
Orientation	$\alpha_a = 130^\circ$ southeast, $\beta = 30^\circ/35^\circ$

Jan.	Feb.	Mar.	Apr.	May	June	July	Aug.	Sep.	Oct.	Nov.	Dec.
0.80	0.80	0.60	0.40	0.20	0.20	0.20	0.20	0.20	0.30	0.50	0.70

Figure 5.12: Monthly values of albedo used in the simulaton of the Grøndalen PV system

After talking to Karl Andreassen it was found that most of this difference is due to the local grid not having the capacity to receive the power from the PV system. When this is the situation the voltage experienced by the inverters increases, and to protect themselves from over-

voltage the inverters shut down automatically. At the website where logged data was retrieved from error messages indicating this have been frequent since march, and about 10 MWh (!) is estimated to have been lost this way. Adding 10 MWh to the measured yield increases the annual specific yield to 894.4 kWh/kWp, or only 4.2 % lower than estimated annual yield.

As the points in time when production has been shut down and what inverters were shut down has not been investigated, it is hard to say anything about the differences in specific yields between the two tilt angles shown in 5.13c and 5.13d. From these plots it can be concluded that the subsystem tilted 35° had a specific yield of 740.2 kWh/kWp while the modules tilted 30° had a specific yield of 804.6 kWh/kWp. From the given data it is evident that this is due to the modules with a tilt angle equal to 30° having had higher yields in the afternoon hours in the period april - august.

Table 5.7: Technical data on the Solar Frontier 165-S module, from [34]

Technology	CIS
Efficiency, η	13.4%
Nominal power, P_N	165 W
STC MPP current/voltage	1.93 A/85.5 V
Temp. coefficient of P_N	$-0.31\%/^\circ\text{C}$
Module area	1.23 m^2

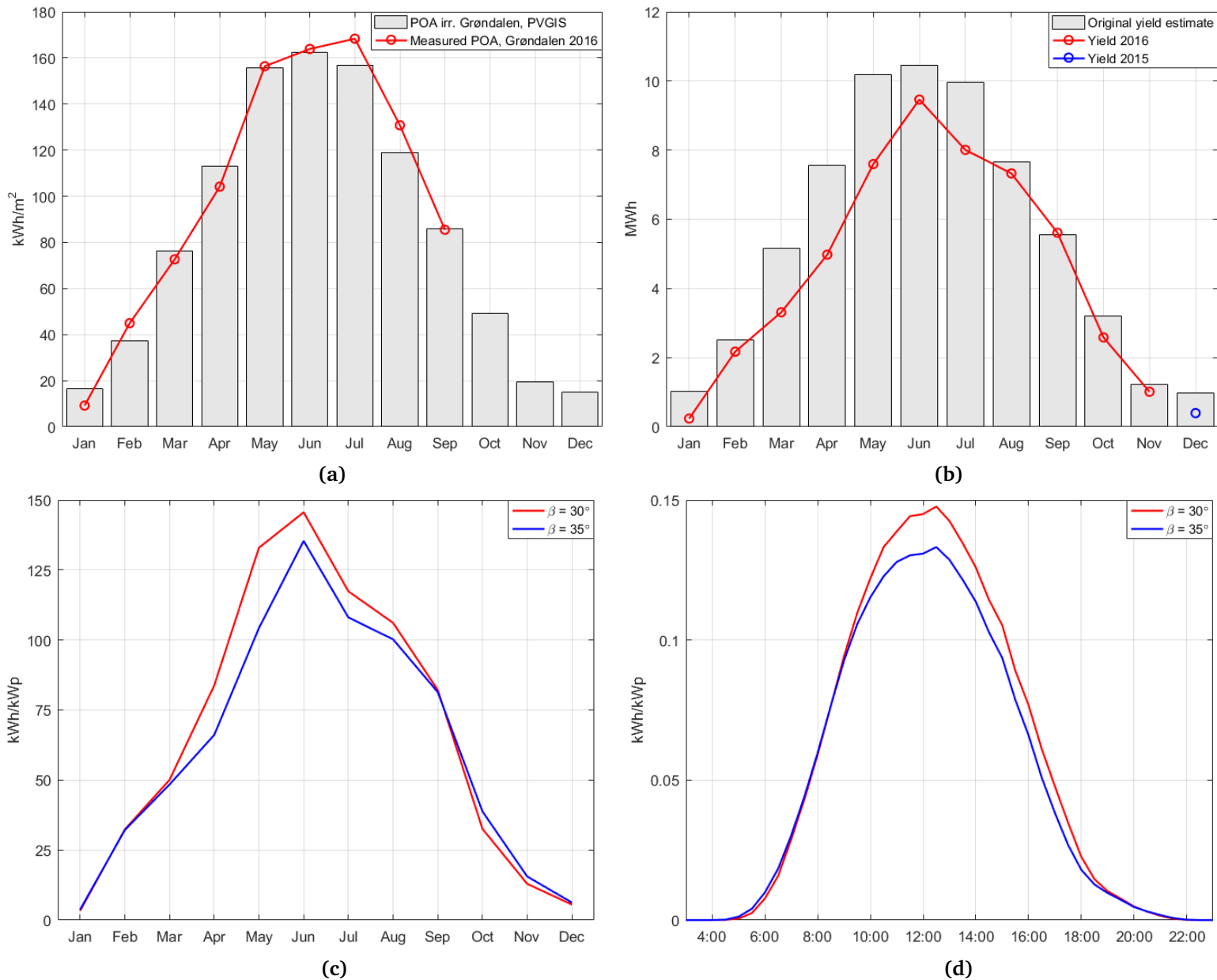


Figure 5.13: Measured and expected irradiation and yield, in addition to average monthly and hourly specific yields, POA irradiation data gotten from Karl Andreassen, Green Energy A/S

Lastly it has been observed that small but slowly declining yields have occurred in the evening hours from about 18:00 until 22:00. This is likely to be caused by the fact that the system is facing southeast, experiencing shading from the roof it is mounted on when the Sun moves far enough westward. As shown in

figure 5.14, this effect is noticeable for almost all months.

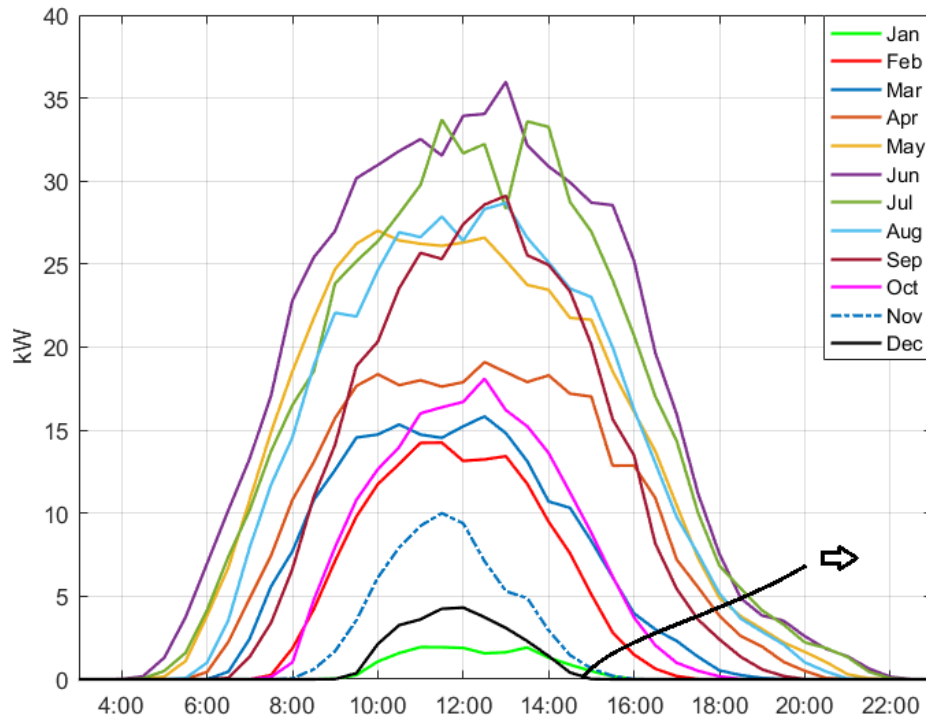


Figure 5.14: Average hourly specific yields at Grøndalen for each month, showing the shading effect

5.4 Powerhouse Kjørbo, Sandvika

At 312 kWp the biggest PV system looked at in this thesis by far lies in Sandvika, about 13 km west of Oslo. It is part of the first project by energy-plus-house organization Powerhouse, which is aiming to show that energy-plus-houses are possible in Norway. The two office buildings at Sandvika that are now energy-plus-houses were originally built in the 80's when construction standards were nowhere near what they are today. Using geothermal heating and solar power the buildings are estimated to have a net

Table 5.8: Technical data on the SunPower SPR-327NE-WHT-D module, from [36]

Technology	mono-Si
Efficiency, η	20.1%
Nominal power, P_N	327 W
STC MPP current/voltage	5.98 A/54.7 V
Temp. coefficient of P_N	-0.38%/°C
Module area	1.63 m ²

energy budget of 3.2 kWh/m²/year, or about 200 kWh/m² produced over the course of their 60 year lifetime.



Figure 5.15: Part of the Powerhouse Kjørbo PV system, photo: Sigurd Øygarden Flæten

Considering the 5180 m² of office space etc. this sums up to a production of about 1 GWh. These estimates have taken into account both what energy was used during renovation, energy bound in materials and energy that will be used for heating, lighting etc. [35]. The PV system at Kjørbo is divided into three parts: One on the roof of each office building and a third on the roof of a nearby garage. All parts are installed at a tilt angle of $\beta = 10^\circ$, but have different azimuth angles. On the office buildings the modules are facing southeast/northwest while they're facing southwest/northeast on the garage roof. Further details on the modules and system are given in table 5.8 and 5.9.

Table 5.9: The system at Powerhouse Kjørbo

	Garage	Building 4/5
Modules	562 x SunPower SPR-327NE-WHT-D	212/180 x SunPower SPR-327NE-WHT-D
Nominal power	183.8 kWp	69.3 kWp/58.9 kWp
Inverters	8 x SMA STP17000TL-10	4 x SMA STP15000TL-10 / 4 x SMA STP12000TL-10
Orientation	$\alpha_a = 70^\circ/250^\circ$ (northeast/southwest), $\beta = 10^\circ$	$\alpha_a = 145^\circ/325^\circ$ (southeast/northwest), $\beta = 10^\circ$
Price	About 5.83 million NOK including transport and installation, or roughly 18.7 NOK/Wp	

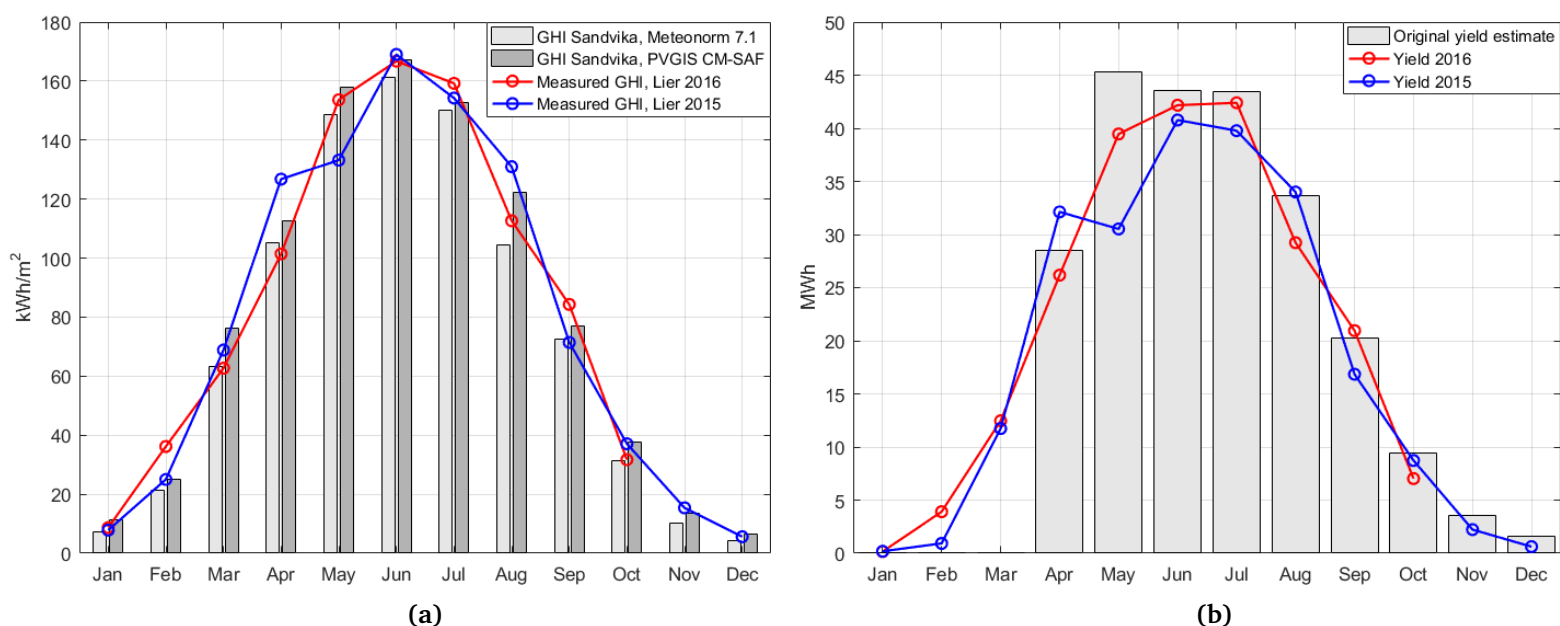


Figure 5.16: Measured and expected yield and irradiation at Powerhouse Kjørbo, measured GHI data from lmt.bioforsk.no

Monthly irradiation and yield is shown in figure 5.16. Lier, lying about 18.3 km from Kjørbo, was again where the nearest measurements of irradiation were found. Comparisons of irradiation and yield may thus not be the most accurate here, but there seems to be rather a high correlation between the two. An exception is June, when the irradiation in 2015 was higher than that in 2016 but the yield behaves oppositely. From this comparison it can be concluded that the low yield of May 2015 seems to have been caused mainly by low irradiation. When going through the hourly yield data it was also found that data was missing/not complete for the two first weeks of May. It should be noted that estimates of irradiation at Sandvika from PVGIS are pretty similar to the measurements from Lier.

In 2015 the yield of the entire Powerhouse Kjørbo PV system was 218.5 MWh, 4.7 % lower than the expected 229.4 MWh. In the period January - October 2016 the total yield was 223.9 MWh, only 0.1% lower than the estimated yield in the same period. This makes the specific yield of the entire system 700.2 kWh/kWp for 2015 and 717.8 kWh/kWp for the 2016 period with data. The yield estimates were obtained from Peter Bernhard at Asplan Viak but were performed by the supplier of the PV system, Swedish company Solkompaniet AB. According to Bernhard the yield in January, February and March were all set to zero to compensate for losses caused by ice and snow. Further details on the simulations were unfortunately not obtained.

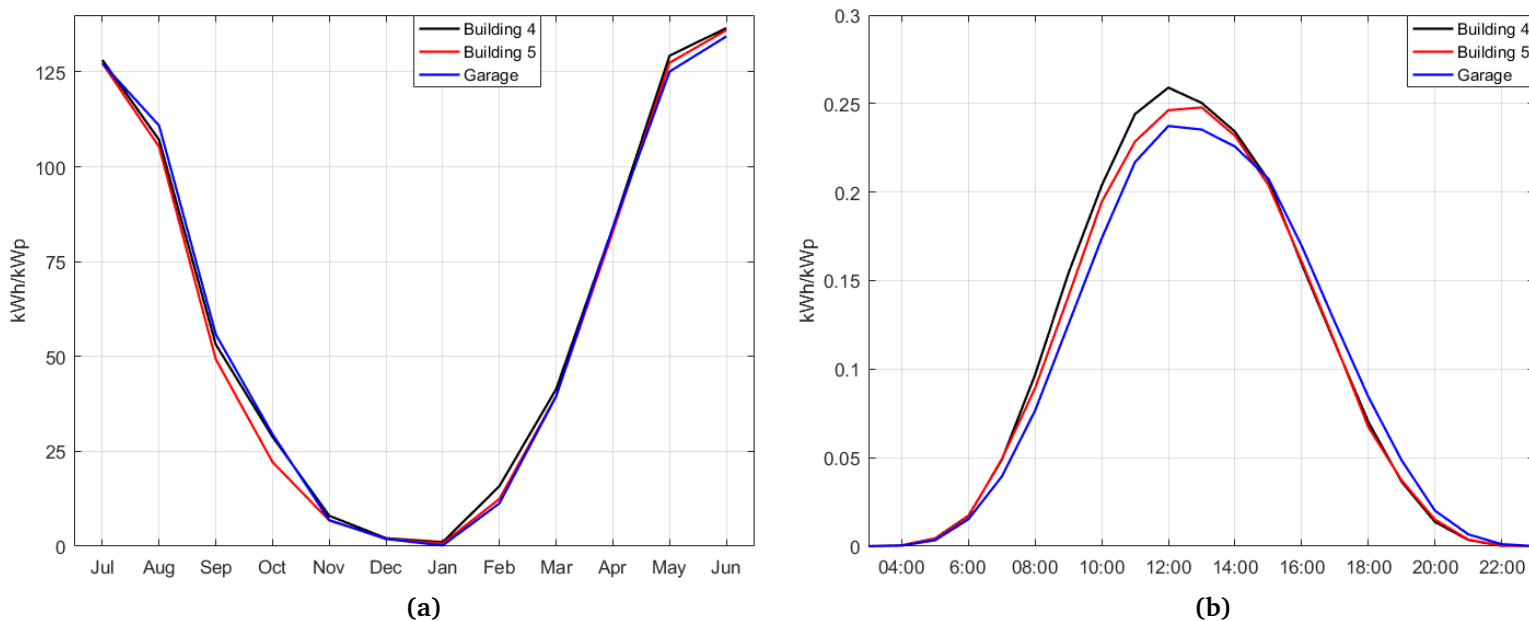


Figure 5.17: Monthly and average hourly specific yields of the different parts of the Powerhouse Kjørbo PV system

As seen in figure 5.17 the specific yields of the different subsystems do not differ substantially, neither on a monthly or hourly basis. Production from the garage roof is shifted slightly towards afternoon hours relative to the other parts of the system. The monthly yields in figure 5.17a from the period July 2015 - June 2016 were chosen because the least missing/incomplete data was found here. Average hourly specific yields in figure 5.17b are taken over the period March 2015 - June 2016, periods with incomplete data having been removed.

5.5 Kiwi Fjeldset, Elverum

Finished in February 2016, the PV system on this grocery store consists of near horizontal modules on the roof, modules mounted vertically on one of the facades of the building and a battery bank. The total nominal power of the system is 94 kWp while the batteries are capable of storing 48 kWh. Additionally, the store offers charging of electric bikes and cars, and reuse of heat from coolers has been estimated to save the owners 85 MWh per year [37].



Figure 5.18: The roof and facade at Kiwi Fjeldset, photos from [37] and [38]

Estimated and measured monthly irradiation and yield is plotted in figure 5.19. At Ilseng, about 21.5 km from Fjeldset, the nearest available irradiation measurements were found. Yield data for the three first weeks of february and the two first weeks of june are unfortunately missing. Periods with missing data are plotted using dashed lines.

Table 5.10: The system at Kiwi Fjeldset

	Roof mounted	Facade
Modules	352 x IBC PolySol 260CS	9 x ISSOL Cenit 220 Model 270
Nominal power	91.52 kWp	2.43 kWp
Inverters	4 x SMA STP 20000TL-30	SMA SB 2.5 1VL-40
Orientation	$\alpha_a = 110^\circ/290^\circ$ (southeast/northwest), $\beta = 10^\circ$	$\alpha_a = 200^\circ$, $\beta = 90^\circ$

The total yield in the period march - november was 58.3 MWh, about 83% of the expected 70.1 MWh. If a crude guess is to be taken on the basis of the irradiation measurements from Ilseng, the yield in june should have been around 13-14 MWh. Assuming the june yield was 13 MWh raises the actual yield to about 93% of expected yield and gives a rough estimate of 691.5 kWh/kWp for the annual specific yield of the entire system. The vertically mounted modules produced 1.05 MWh alone. If one accounts for the missing data in june and assumes that the yield here was about 154 kWh, the specific yield of vertical modules ends up at 465 kWh/kWp. The specific yield of the roof mounted system in this period has been 624.4 kWh/kWp based on the raw data, but is 696.7 kWh/kWp when corrected. Production in january, february and december will raise these values

somewhat, but the low yield in november suggests this is a good approximation of the annual specific yields.

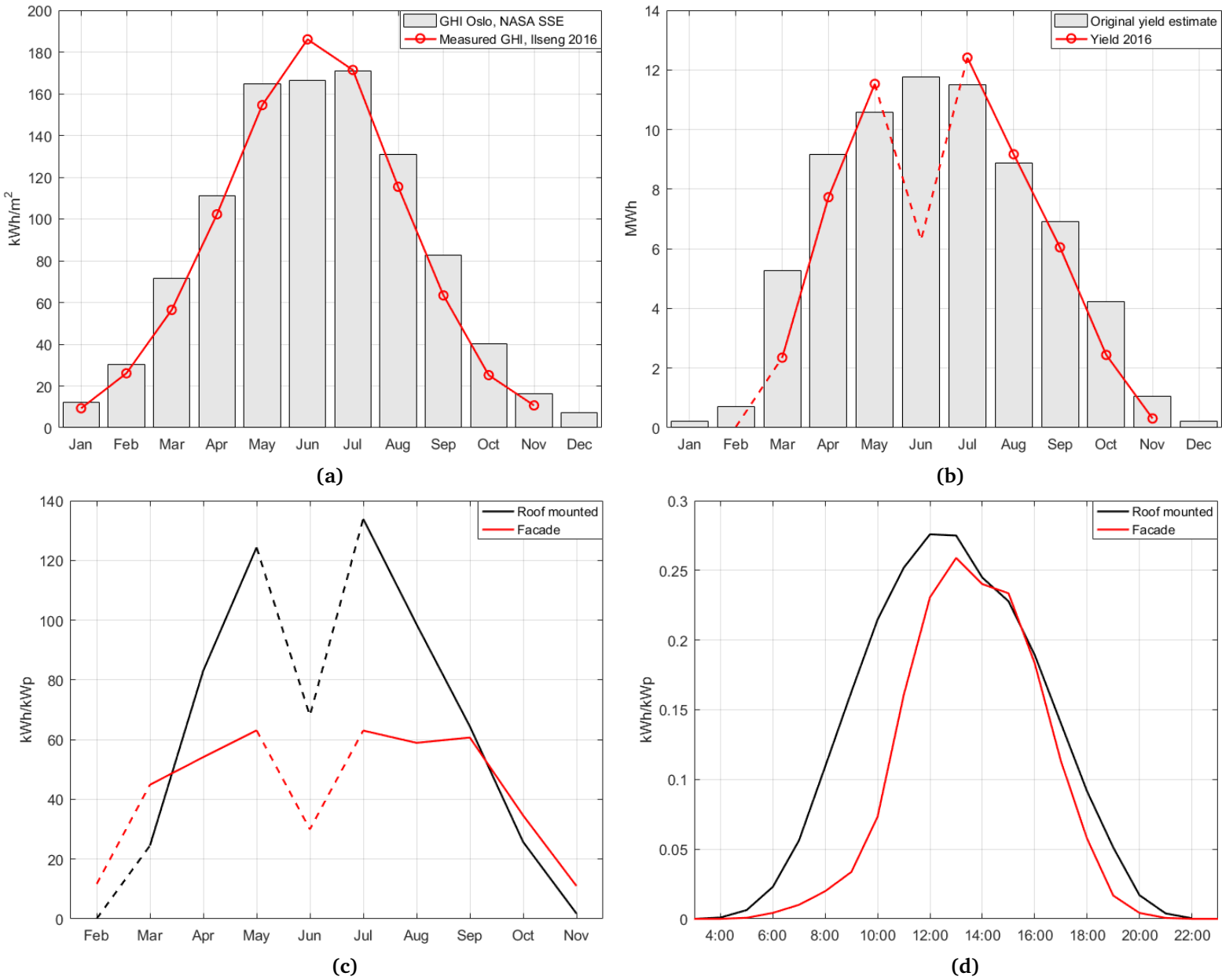


Figure 5.19: Expected and measured irradiation and yield at Fjeldset in addition to monthly and average hourly specific yields, dashed lines indicating periods with missing data. Measurements of GHI gotten from lmt.bioforsk.no

Overall the spring and fall months must be said to be a disappointment when

compared to simulations. There are too many unknown factors to say anything with certainty about the performance of this system compared to simulations so far. The simulation of the roof system was performed by supplier FUSen using IBC's solarcalculator. The source of irradiation data used here is unknown, but again NASA has been mentioned as possible. Any further details about the simulation is unfortunately not known to the author. Irradiation has been measured at the system site from october 27th and onwards, hopefully making it possible to evaluate the performance of the system in more detail in the future.

Figure 5.19c shows that about a week of operation in february was enough to reveal the difference in specific yield between the vertical modules and those mounted on the roof. It should also be noted that, being mounted vertically, and therefore not having to deal with snow to the same degree as the roof mounted modules may also have played a role in increasing the difference between the subsystems both in february aswell as march. As seen in figure 5.20, almost no yield was gotten from the roof mounted modules in the periods 24/2 - 8/3 and 25/3 - 31/3 while the yield from the vertically mounted modules kept rising fairly steady in the same periods. At least the latter of these production pauses could be solely caused by snow cover, while the former delay of production could be a combination of snow cover, low solar height or just errors with data logging/the inverters. April did not have any pauses like the ones described here. Hourly average specific yields in figure 5.19d show a rather narrow period of production with a peak at 13:00 for the vertical modules, and a broader one for the roof mounted modules.

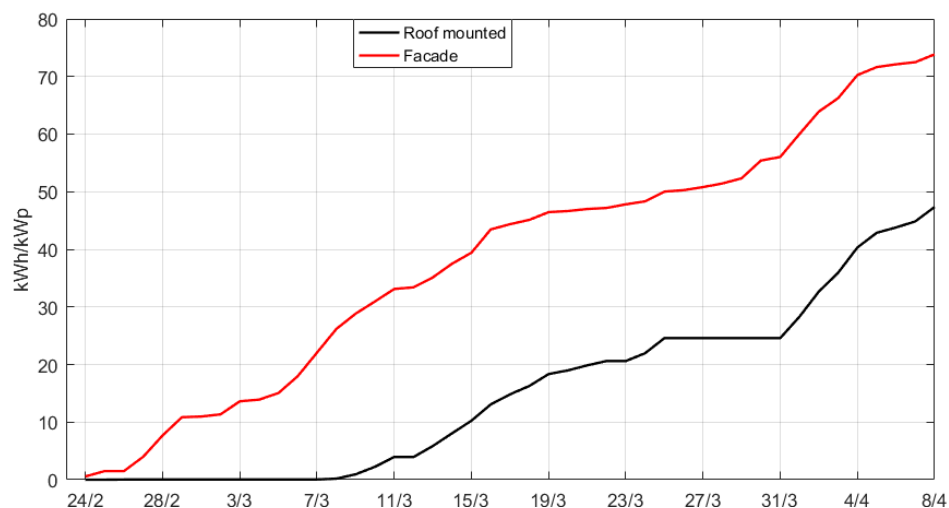


Figure 5.20: Cumulative specific yield at Kiwi Fjeldset

5.6 Other systems

5.6.1 Longyearbyen, Svalbard

In 2013 the first grid-connected PV system was installed on Svalbard and as seen in figure 5.21 it performed much better than expected. The yield estimates were done by supplier Solbes AS and were based on average meteorological data from Svalbard. Even with four months of zero yield the annual specific yield ended up at 621 kWh/kWp. Because of high electricity prices on Svalbard it has been estimated that PV systems can be fully paid back within 6 years here and compete with other energy sources [71].

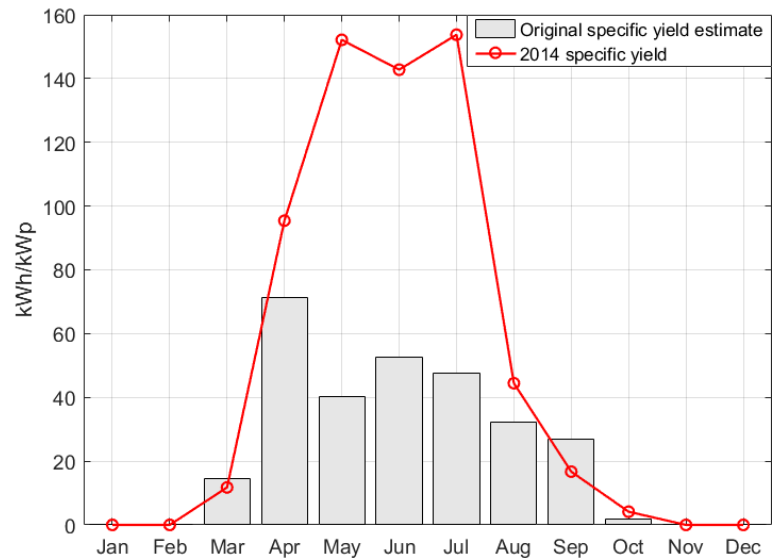


Figure 5.21: Part of the system at Longyearbyen and its monthly specific yield, photo and data gotten from Solbes AS

5.6.2 "Låven" - Hedmark College, Evenstad

The roof of this campus building was installed with a 70.4 kWp PV system in late 2013. The average annual specific yield has been 889 kWh/kWp, slightly better than the expected 853 kWh/kWp.

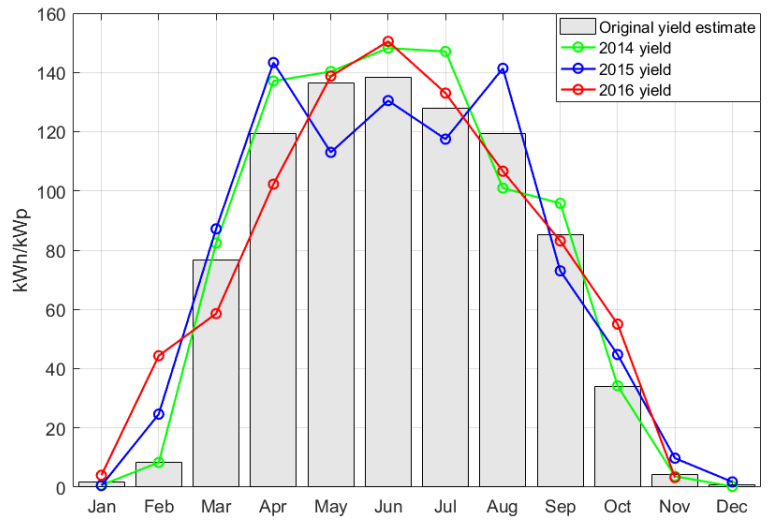


Figure 5.22: The roof mounted system at Evenstad and monthly its specific yield, photo by Statsbygg/Tove Lauluten and data from sunnyportal.com

5.6.3 Oseana, Os

Finished in late 2011, almost 5 years of yield data exist on this 63.5 kWp mono-Si PV system in Os. It is a fully integrated system with tilt angles varying from near vertical to near horizontal. Average annual specific yield lies at 803.6 kWh/kWp. Data on expected yield was unfortunately not found.

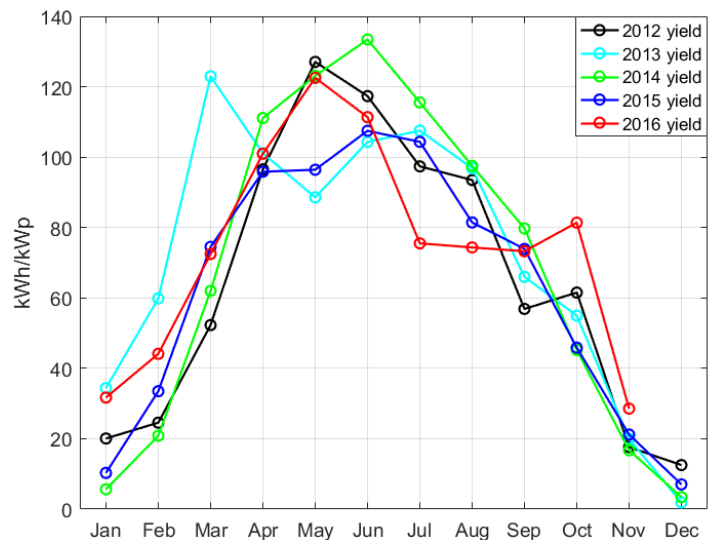


Figure 5.23: Part of the Oseana system and its specific yield, photo by Aasa Christine Stoltz and data from sunnyportal.com

5.7 Summary

Generally speaking, the performance of three types of PV system orientations has been studied in this chapter: The east/west solution where modules are tilted 10° and are facing opposite directions, modules tilted about 30° facing southwards and vertically mounted modules facing various directions. Looking at annual specific yields, or specific yields in the periods where data exists, reveals that the east/west systems actually perform quite similarly: About 700 kWh/kWp/year seems like a good approximation for all of them even though they are facing in somewhat different directions and are located in different parts of the country. Regarding snow cover losses on these nearly horizontal systems some periods of zero yield are observed, particularly in february/march.

Systems with larger tilt angles, like 30° and 35° at Grøndalen, have substantially higher specific yields. Based on this system and the system at Evenstad, slightly above 900 kWh/kWp/year seems average. The system at Grøndalen was also the only system consisting solely of CIGS modules and can be said to have performed roughly the same as the c-Si system at Evenstad. Uncertainties regarding actual yield at Grøndalen caused by losses due to lacking grid capacity make a detailed comparison difficult.

The vertically mounted systems studied here are varying most in performance. Losses from shading have substantially decreased the yield of two of the facades at Solsmaragden, while the southwestern facade, not affected by this, performs almost as well as the roof mounted subsystem at the same location. Neglecting losses from the green print that is covering all of the Solsmaragden facades puts the annual specific yield of these vertical modules above 700 kWh/kWp . The other vertically mounted systems studied here have annual specific yields of $300 - 450 \text{ kWh/kWp}$, including the south-facing modules at Fjeldset. Evaluating the location and orientation of a system that is to be installed vertically can thus be argued to be of extra importance.

Regarding the precision of yield estimates, a deviation of about 5% between measured and predicted values is average for the cases that are looked at here. Deviations from expected irradiation seems to be the main cause this difference, but exact sources of meteorological/irradiation data used in simulations are unfortunately only known for the estimates performed for the systems at Haakonssvern and Grøndalen Gård.

/6

Sensitivity analyses

Lastly some simulations of how various orientations of PV systems perform at different locations were performed. The gathered hourly data on global/diffuse irradiation from NTNU, UiB and NMBU in addition to temperature averages over 10 years from nearby locations were used as input. Irradiance data was supplied by Jan Olseth, Oddbjørn Grandum and Signe Kroken at UiB, NTNU and NMBU respectively. Temperature data was gotten from MET (eklima.no), where measurements from the same locations as where irradiation was measured was available at Bergen and Ås, while temperatures from Voll, about 2 km from the NTNU Gløshaugen campus, were used with the NTNU data. The periods of which the irradiation averages were taken over are shown on figure 6.1. Regarding incomplete data 1.6% were missing of both the global as well as diffuse measurements from NTNU, 1.5% and 1.1% were missing of the global and diffuse measurements from UiB respectively and lastly 0.2% were missing of the data on both the global as well as the diffuse irradiance from NMBU.

A total of six applications/orientations were simulated at each location. Orientations were chosen to be a mix of what is and might be likely to be installed in Norway. Equation 2.15 was considered as a basis for optimal tilt angles at each location, but PVsyst has a tool which calculates optimal tilt- and azimuth angles based on irradiation data as well. Comparing the two, the largest difference in optimal tilt angle was gotten for Bergen where equation 2.15 gives $\beta = 48.3^\circ$ while PVsyst calculates an optimum at approximately $\beta = 40^\circ$. Likewise, the difference at Trondheim is 6.0° and 2.7° at Ås, tilt angles from equation 2.15

being larger in each case. As seen in figure 6.1, the

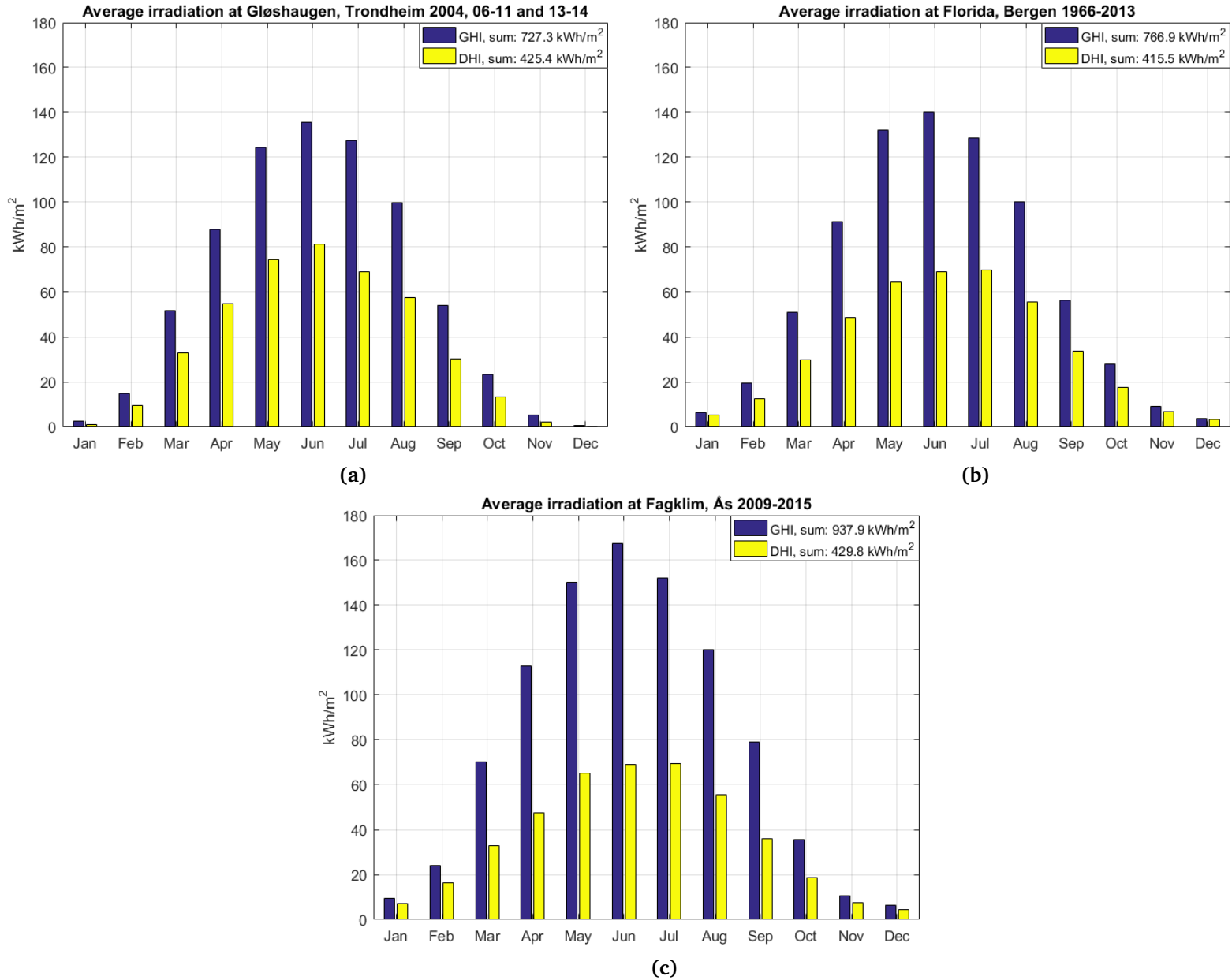


Figure 6.1: Monthly average irradiation at Trondheim, Bergen and Ås

annual sum of DHI at each location is in fact similar and the amount of direct irradiation is what separates them. Since PVsyst takes into account this direct/diffuse ratio these estimates should be more representative of real conditions. Optimal tilt angles from PVsyst were thus used in the simulations

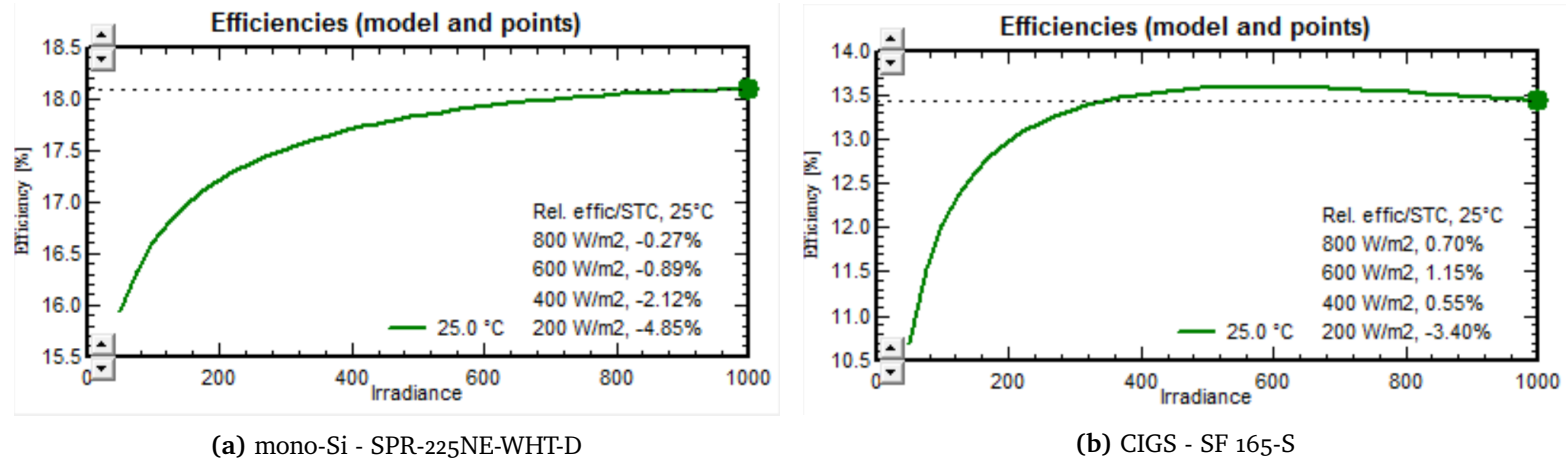


Figure 6.2: Low-light efficiencies of the two modules used in the simulations

and for Trondheim, Bergen and Ås these were calculated to be approximately 45°, 40° and 45° respectively.

The simulations were all based on 4.95 kWp systems oriented in one direction, except the east/west ($\alpha = \pm 90^\circ$) solution where half of the modules were facing each way. The CIGS modules used are identical to those installed at Grøndalen Gård, the Solar Frontier 165-S, while details on the mono-Si module from SunPower used are specified in table 6.1. Since efficiencies of the two technologies differ somewhat, 22 mono-Si modules and 30

Table 6.1: Technical data on the SunPower SPR-225NE-WHT-D module, from [36]

Technology	mono-Si
Efficiency, η	18.1%
Nominal power, P_N	225 W
STC MPP current/voltage	5.62 A/40.0 V
Temp. coefficient of P_N	-0.37%/°C
Module area	1.24 m ²

CIGS modules had to be used to end up at 4.95 kWp. This also illustrates the fact that c-Si modules produce more per m², which again can be an important factor when considering what system to buy. Since shading effects are completely neglected in all simulations performed in this chapter, the actual area use of systems with multiple rows of modules is therefore not possible to calculate. For simplicity the area used by each system is thus not looked at here. How PVsyst models the low-light performance of these two models based on IV-curves from the manufacturers is shown in figure 6.2. As shown in table 5.7 and 6.1 the temperature coefficients of the two modules differ, but only by 0.06%/°C. The final factor that separated the two technologies in the simulations was that a 2% gain in yield was added to the CIGS system as a result of light-soaking. LID effects for the mono-Si system and general

degradation of both systems were neglected. IAM losses were set to default values, the factor b_0 in equation 3.3 being 0.05. Regarding thermal loss factors, these were set to different values for different orientations. To simulate reduced heat transfer from the back of the modules, the constant thermal loss factor U_c was set to 15 W/m²K for the vertical systems. According to PVsyst this is representative of "integration with fully insulated back". For the horizontal system U_c was set to 20 W/m²K and for the rest of the orientations it was set to 29 W/m²K, representative of systems being "semi-integrated with air duct behind" and having "free mounted modules with air circulation" respectively. To simulate differences in how long snow cover would be able to stay on each system orientation, different values of soiling losses were used. Although there are differences in the climates at Trondheim, Bergen and Ås, differences in soiling losses between locations were neglected. For the horizontal systems soiling losses were set to 4%, for the systems tilted 10° they were set to 2%, for systems at 30° or optimal tilt angle they were set to 1% while vertical systems were simulated with no soiling losses. Lastly, the transposition models of Hay and Perez were used in each case to reveal any differences. The outcomes of the simulations are shown in figure 6.3.

What might be apparent at first is the rather constantly higher yield from the CIGS systems. Although maybe not visible in figure 6.3 there were varying differences in the performance of each technology at the three locations. The differences caused by temperature and irradiance level when simulated at optimal tilt angle using the Hay transposition are shown in figure 6.4. The values at the bottom arrows in each subfigure are the amounts of energy that PVsyst would subject to further losses, such as inverter and ohmic losses. Even though much of the differences between CIGS and mono-Si in figure 6.3 are a result of the constant gain of 2% from light soaking, the CIGS systems actually out-performed the mono-Si systems without it as well. Without light soaking the numbers for the CIGS systems are 4172 kWh, 4239 kWh and 5.51 MWh at Trondheim, Bergen and Ås respectively. Also evident from the figure is that you get substantially less for tilting your modules in Bergen than one might expect from just the latitude of the location, as seen in each subfigure as the item "global incident in coll. plane". Using the Perez transposition raises the yield increase from tilting optimally at each location to 27.9%, 25.3% and 36.6% at Trondheim, Bergen and Ås respectively. Ås and Bergen lie at pretty much the same latitude (59.66° N and 60.39° N respectively), but the differences in the ratio direct/diffuse irradiation causes tilting to give much less of a yield increase in Bergen than in Ås. In fact, every orientation simulated here gave less of a relative increase in yield compared to horizontal yield than in both Trondheim and Ås. The vertical and east/west orientations gave the largest relative increases in yield in Trondheim while the systems tilted 10°, 30° and optimally facing south all gave the largest increases in Ås. These results were gotten with both transposition models.

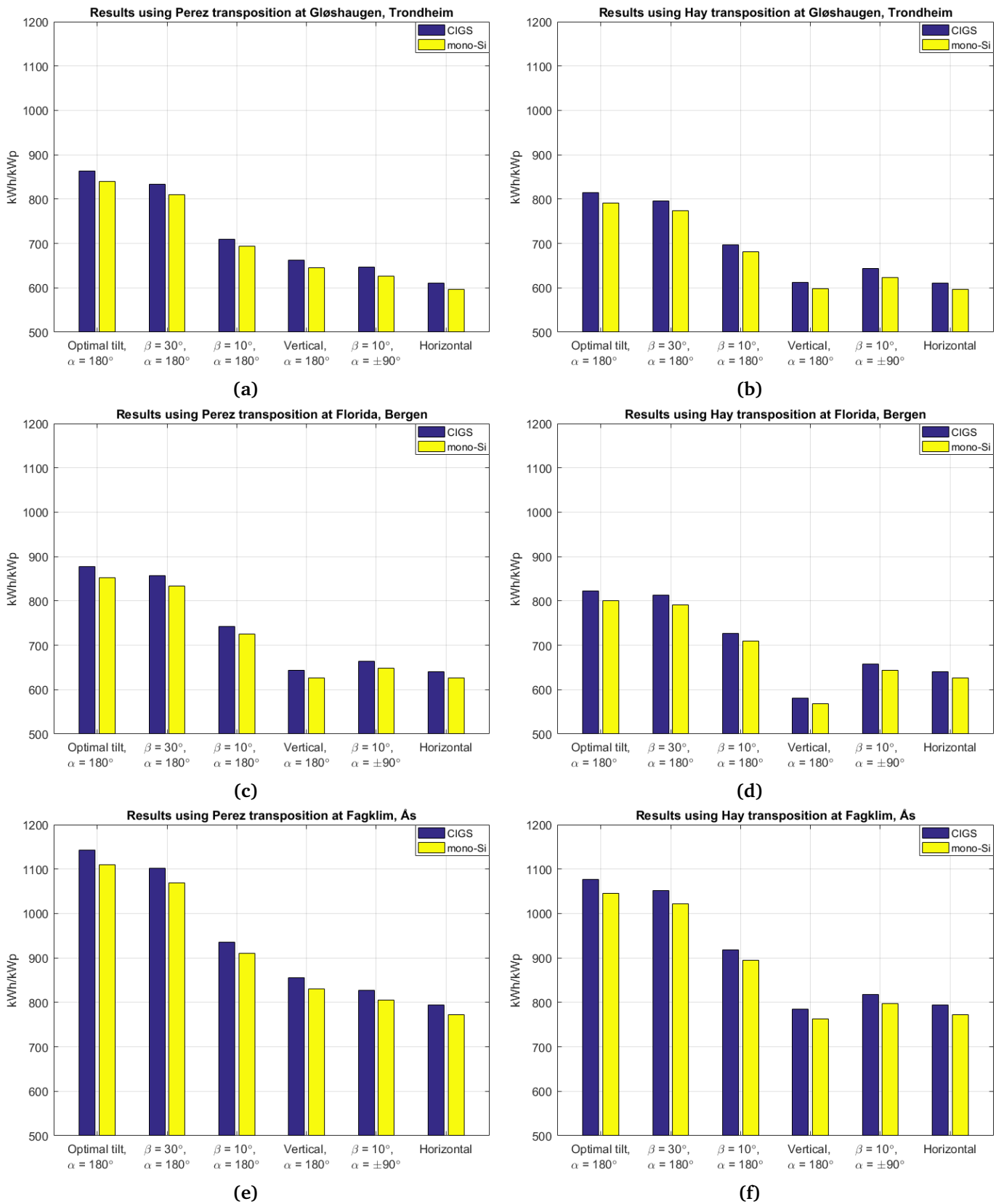
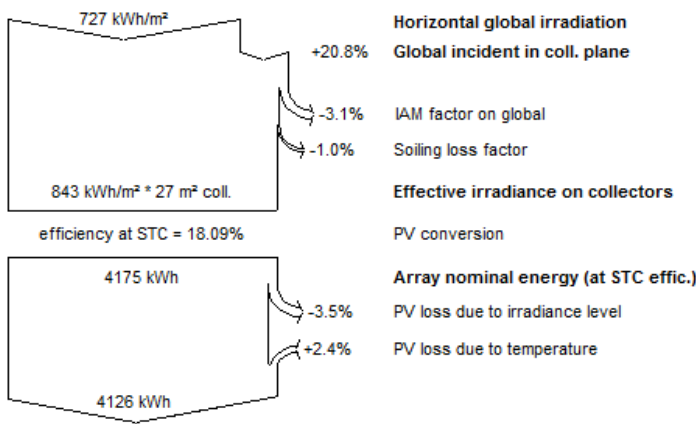
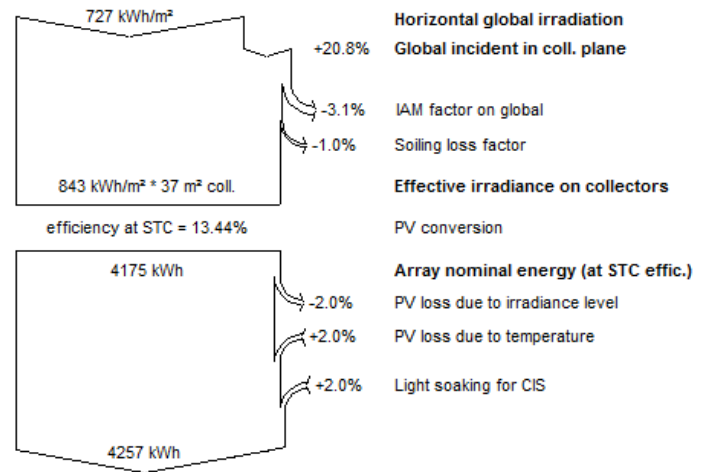


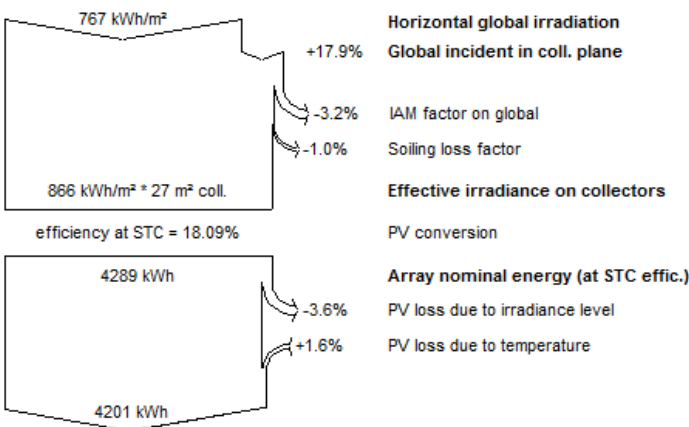
Figure 6.3: Annual specific yield results for different orientations at the three locations



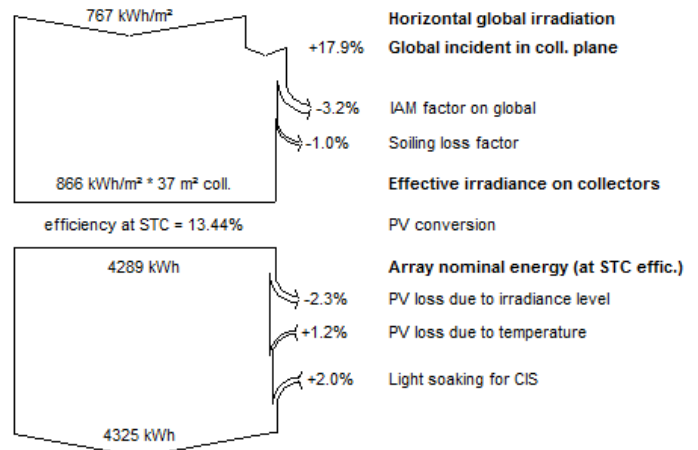
(a) mono-Si, Trondheim



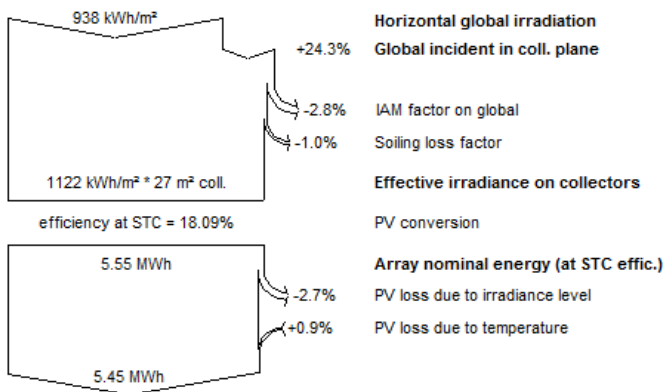
(b) CIGS, Trondheim



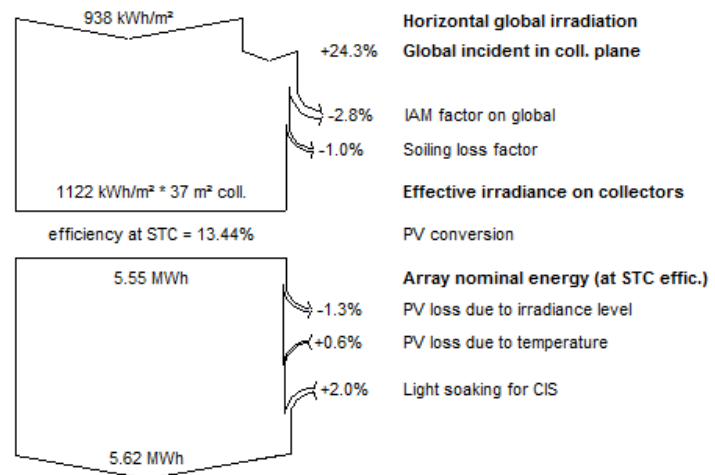
(c) mono-Si, Bergen



(d) CIGS, Bergen



(e) mono-Si, Ås



(f) CIGS, Ås

Figure 6.4: The effect of irradiance levels and temperature, simulated at optimal tilt angles at each location with the Hay transposition model

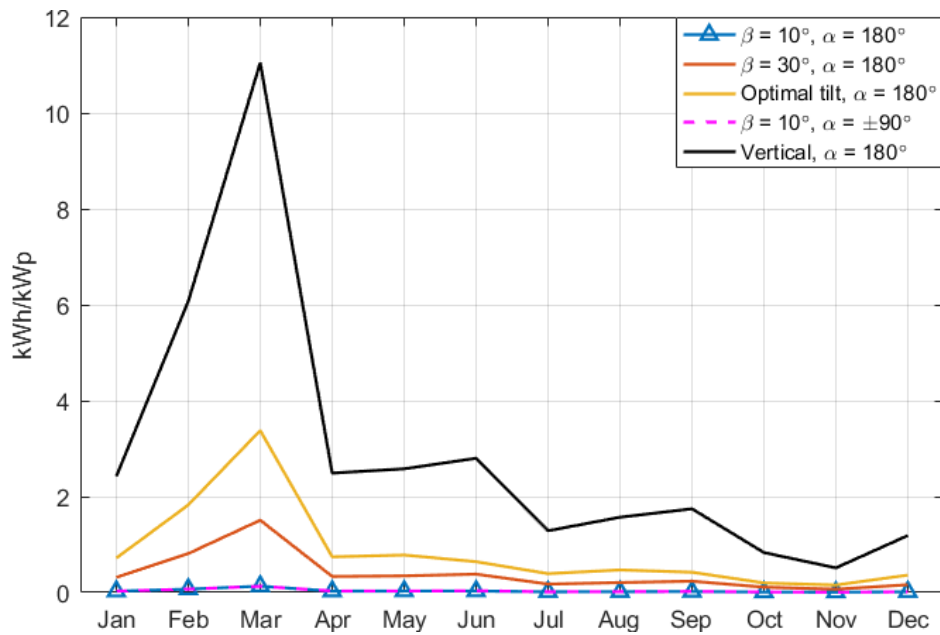


Figure 6.5: Differences in monthly specific yield at Ås, using the Perez transposition model and two sets of monthly albedo values

To look at what effect higher albedo had on the yield of different orientations, the average monthly measured albedo values shown in figure 4.2 from Ås were used in simulations of the different orientations. Comparing these results to the simulation where the standard value of 0.2 was used for every month show that march is the month of highest yield gain caused by albedo change. Not surprisingly, the vertical system has the highest gain in yield caused by this change over the whole year. Some attempts at implementing the Sandia model with spectral corrections as depicted in figure 3.2 were also made, but for reasons unclear to the author no changes in simulations occurred.



Conclusions and further work

Irradiation data from 57 stations has been gathered and confirm that annual irradiation in Norway lies at 700 - 1000 kWh/m². Calculating RMS errors for the three irradiation models/databases Meteonorm 7.1, PVGIS and NASA SSE reveal that the former two perform about similarly while the latter has a higher error. Due to the differences in resolutions this is not surprising. When used at specific locations a quick check should be done to see what model works best here, as rather large local errors are observed. Further analyses of how different irradiation models perform in Norway should be done in order to improve the precision of PV yield simulation. Data on diffuse irradiation has been gathered from the locations of Trondheim, Bergen and Ås and show that 58.5%, 54.2% and 45.8% of GHI is diffuse irradiation respectively.

The performance of several PV systems in Norway has been looked at in this thesis, mainly in terms of annual specific yield. It has been found that systems installed using the so-called east-west solution perform relatively similarly. The yield of three such systems located at around 60° north have been analyzed, and results show annual specific yields at about 700 kWh/kWp. A system consisting of CIS/CIGS modules has also been look at, but due to large losses caused by the local grid lacking capacity it is difficult to state anything precise about the performance of this technology. Nonetheless it seems to have performed roughly like a crystalline silicon system of the same size.

Modules installed vertically have also been investigated and show potential equal to those applications where east/west solutions have been used. Large variations in performance are observed though, especially due to losses caused by shading and suboptimal locations/orientations. As expected these systems perform better in winter months but tend to have narrower periods of production over the course of a typical day.

Lastly an analysis on how different PV applications can be said to generally perform at different locations in Norway has been done. Results show that the increase in yield gotten from tilting a system, compared to the yield of a horizontal system, is the lowest in Bergen. Also, you get the highest relative increase using the east/west solution ($\beta = 10^\circ$) and a system tilted 10° facing south in Trondheim. At Ås the highest relative increase in yield gotten for systems tilted 30° and optimally (45°) is observed.

Thus the conclusion is that a well designed PV system has great potential also in Norway. A further decrease in the prices of PV in Norway as a result of decreasing global prices and a maturing Norwegian market will most likely make PV systems a viable option for lowering the electricity bill for Norwegians.



The Perez Sky Diffuse Model

The Perez model is summarized in equation 2.9, but the coefficients and functions are calculated as follows:

$$a = \max(0, \cos\theta) \quad (\text{A.1})$$

$$b = \max(\cos(85^\circ), \cos\beta) \quad (\text{A.2})$$

$$F_1 = \max(0, (f_{11} + f_{12}\Delta + \frac{\pi\phi}{180^\circ}f_{13})) \quad (\text{A.3})$$

$$F_2 = f_{21} + f_{22}\Delta + \frac{\pi\phi}{180^\circ}f_{23} \quad (\text{A.4})$$

$$\Delta = \frac{DHI \cdot AM_a}{G_{ex}} \quad (\text{A.5})$$

Here, G_{ex} is the extraterrestrial radiation and AM_a the absolute air mass given by

$$AM_a = AM \cdot \frac{P}{P_0} \quad (\text{A.6})$$

where P is the given pressure while P_0 is the standard pressure of 1 atm. The extraterrestrial radiation is gotten by taking into account the variations around the solar constant

$$G_{ex} = 1366.1 \cdot \left(\frac{R_{av}}{R}\right)^2 \text{ W/m}^2 \quad (\text{A.7})$$

where R_{av} is the average Sun-Earth distance and R is the actual distance. This ratio can again be expressed as [19]

$$\left(\frac{R_{av}}{R}\right)^2 = 1.00011 + (0.034221 \cdot \cos(c)) + (0.000128 \cdot \sin(c)) \\ + (0.000719 \cdot \cos(2c)) + (0.000077 \cdot \sin(2c)) \quad (\text{A.8})$$

$$c = 2\pi \cdot \frac{N}{365} \text{ radians} \quad (\text{A.9})$$

where N is the day number. The coefficients in equations A.3 and A.4 are lastly determined by what interval the so-called clearness ϵ lies in, which is given by

$$\epsilon = \frac{((DHI + DNI)/DHI) + (\kappa\beta^3)}{1 + (\kappa\beta^3)} \quad (\text{A.10})$$


where κ is equal to 1.041 when the tilt angle is given in radians and $5.535 \cdot 10^{-6}$ when it's given in degrees. The coefficients are then decided according to the following two tables:

Table A.1: Intervals for ϵ bins

ϵ bin	Lower bound	Upper bound
1 (Overcast)	1	1.065
2	1.065	1.230
3	1.230	1.500
4	1.500	1.950
5	1.950	2.800
6	2.800	4.500
7	4.500	6.200
8 (Clear)	6.200	—

Table A.2: Coefficients for each ϵ bin

ϵ bin	f_{11}	f_{12}	f_{13}	f_{21}	f_{22}	f_{23}
1	-0.008	0.588	-0.062	-0.06	0.072	-0.022
2	0.13	0.683	-0.151	-0.019	0.066	-0.029
3	0.33	0.487	-0.221	0.055	-0.064	-0.026
4	0.568	0.187	-0.295	0.109	-0.152	-0.014
5	0.873	-0.392	-0.362	0.226	-0.462	0.001
6	1.132	-1.237	-0.412	0.288	-0.823	0.056
7	1.06	-1.6	-0.359	0.264	-1.127	0.131
8	0.678	-0.327	-0.25	0.156	-1.377	0.25



Average annual GHI for some locations in Norway

Table B.1: Gathered global horizontal irradiation data

Location	GHI	Period with data	Data source	MASL	Missing data
Årnes	941	1999 - 2015	LMT, Bioforsk	162	4928 hours, 3.3%
Ås, NMBU	964	97 - 05 and 07 - 15	LMT, Bioforsk	94	2191 hours, 1.4%
Landvik	967	1995 - 2015	LMT, Bioforsk	10	6868 hours, 3.7%
Hokksund	859	92 - 94 and 97 - 15	LMT, Bioforsk	15	5118 hours, 2.7%
Hønefoss	923	92 - 94, 96 - 05 and 08 - 15	LMT, Bioforsk	126	2048 hours, 1.1%
Lier	972	1992 - 2015	LMT, Bioforsk	38	7983 hours, 3.8%
Maze	636	1986 - 1991	MET, klima.no	277	994 hours, 1.9%
Pasvik	692	97 - 05 and 08 - 15	LMT, Bioforsk	27	933 hours, 0.6%
Alvdal	931	1993 - 2015	LMT, Bioforsk	478	2890 hours, 1.4%
Ilseeng	910	92 - 05 and 08 - 15	LMT, Bioforsk	182	3206 hours, 1.7%
Kise	865	96 - 05 and 07 - 15	LMT, Bioforsk	129	2919 hours, 1.8%
Roverud	896	92 - 94, 97 - 05 and 07 - 15	LMT, Bioforsk	172	3783 hours, 2.0%
Etne	807	1997 - 2015	LMT, Bioforsk	8	4775 hours, 2.9%
'Kvam	653	1997 - 2012	LMT, Bioforsk	13	5492 hours, 3.9%
Ullensvang	754	1998 - 2015	LMT, Bioforsk	13	6024 hours, 3.8%
Bergen, Florida	767	1966 - 2013	GFI, UiB	45	4728 hours, 1.1%
Linge	835	1997 - 2015	LMT, Bioforsk	34	3748 hours, 2.3%

Surnadal	777	1993 - 2015	LMT, Bioforsk	5	7205 hours, 3.6%
Tingvoll	774	1997 - 2015	LMT, Bioforsk	23	5541 hours, 3.3%
Myken	774	2015	MET, klima.no	17	13 hours, 0.2%
Sortland	729	93 - 96, 98 - 99 and 01 - 15	LMT, Bioforsk	14	6089 hours, 3.3%
Tjøtta	727	1996 - 2015	LMT, Bioforsk	10	7805 hours, 4.5%
Valnesfjord	679	2015	MET, klima.no	20	213 hours, 2.4%
Vågønes	726	1998 - 2013	LMT, Bioforsk	26	2875 hours, 2.1%
Frosta	834	93 - 05 and 08 - 15	LMT, Bioforsk	18	6417 hours, 3.5%
Kvithamar	803	1996 - 2015	LMT, Bioforsk	28	6812 hours, 3.9%
Mære	760	1992 - 2015	LMT, Bioforsk	59	9403 hours, 4.5%
Skogmo	739	1993 - 2015	LMT, Bioforsk	32	5187 hours, 2.6%
Apelsvoll	848	1996 - 2015	LMT, Bioforsk	262	7226 hours, 4.1%
Fåvang	876	1993 - 2015	LMT, Bioforsk	184	9079 hours, 4.5%
Gausdal	850	1993 - 2015	LMT, Bioforsk	375	7680 hours, 3.8%
Gran	917	1992 - 2015	LMT, Bioforsk	245	8618 hours, 4.1%
Løken	907	1995 - 2015	LMT, Bioforsk	527	4609 hours, 2.5%
Oslo, Blindern	929	1997 - 2005	MET, klima.no	94	353 hours, 0.5%
Hjelmeland	798	1998 - 2015	LMT, Bioforsk	43	1142 hours, 0.8%
Særheim	910	1997 - 2015	LMT, Bioforsk	90	4416 hours, 2.7%
Fureneset	801	1997 - 2015	LMT, Bioforsk	12	6236 hours, 3.7%
Gjengedal	785	1992 - 1995	MET, klima.no	355	556 hours, 1.6%
Njøs	783	92 - 94, 97 - 05 and 13 - 15	LMT, Bioforsk	45	1053 hours, 0.8%
Rissa	818	93 - 05 and 08 - 15	LMT, Bioforsk	23	2965 hours, 1.6%
Skjetlein	820	92 - 94, 97 - 05 and 08 - 15	LMT, Bioforsk	44	877 hours, 0.5%
Trondheim, Voll	714	1997 - 2010	MET, klima.no	127	26 hours, 0.02%
Trondheim, NTNU	730	04, 06 - 11 and 13 - 14	NTNU	72	1645 hours, 2.1%
Bø	914	92 - 94, 97 - 05 and 07 - 15	LMT, Bioforsk	105	2487 hours, 1.4%
Gjerpen	975	97 - 05 and 07 - 15	LMT, Bioforsk	41	2850 hours, 1.8%
Gvarv	901	2005 and 07 - 14	LMT, Bioforsk	94	1811 hours, 2.3%
Tromsø, Holt	656	97 - 07, 2009 and 11 - 15	LMT, Bioforsk	12	5193 hours, 3.5%
Tromsø, UiT	801	1993 - 2015	UiT, weather.cs.uit.no	55	70614 minutes, 0.7%
Kjeviek	932	97 - 99 and 2003	MET, klima.no	12	1 hour, 0.003%
Lyngdal	895	97 - 00 and 05 - 15	LMT, Bioforsk	4	2113 hours, 1.7%
Ramnes	983	92 - 94 and 97 - 15	LMT, Bioforsk	39	3614 hours, 1.9%
Sande	923	97 - 05 and 08 - 15	LMT, Bioforsk	35	905 hours, 0.6%
Sandefjord	900	00 - 13 and 2015	Jotun AS	20	2 months, 1.2%
Tjølling	974	2005 - 2015	LMT, Bioforsk	19	1811 hours, 1.9%
Rakkestad	962	97 - 05 and 07 - 15	LMT, Bioforsk	102	1901 hours, 1.2%
Rygge	962	2014 - 2015	LMT, Bioforsk	35	1 hours, 0.006%
Tomb	995	92 - 94, 96 - 05 and 07 - 15	LMT, Bioforsk	12	4042 hours, 2.1%
Øsaker	967	2005 and 07 - 15	LMT, Bioforsk	45	1530 hours, 1.8%



Tables of measured versus synthetic GHI/DHI

Table C.1: Measured versus synthetic GHI and DHI at Gløshaugen, Trondheim

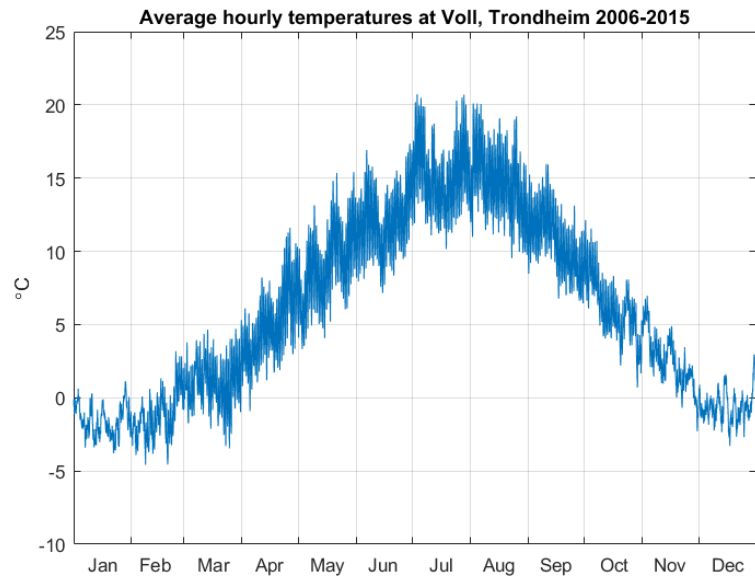
	Meas. GHI	Missing	Meas. DHI	Missing	Meteo GHI	Meteo DHI	SSE GHI	SSE DHI
Jan	2.8	5.2%	1.2	5.2%	5.8	4.0	5.0	4.0
Feb	15.2	0.2%	8.9	0.2%	22.7	10.9	19.3	13.4
Mar	52.0	0.1%	28.3	0.1%	64.4	30.1	57.0	36.0
Apr	88.1	0.4%	44.2	0.4%	110.6	46.6	106.8	57.9
May	124.6	0.02%	56.8	0.02%	153.0	67.5	153.8	76.6
Jun	135.6	0.02%	62.2	0.02%	158.1	84.5	155.7	83.1
Jul	127.9	4.7%	44.5	4.7%	153.6	84.6	144.5	80.3
Aug	100.1	0.8%	42.4	0.8%	112.4	58.5	113.8	67.3
Sep	54.3	0.5%	23.2	0.5%	66.4	35.3	72.0	40.8
Oct	23.6	0.8%	10.6	0.8%	29.5	17.9	32.9	21.4
Nov	5.5	2.4%	0.8	2.4%	8.0	6.0	9.0	6.6
Dec	0.9	9.6%	0.6	9.6%	2.7	2.0	1.9	1.6
Year	730.4	2.1%	323.6	2.1%	887.2	447.9	871.5	488.9

Table C.2: Measured versus synthetic GHI and DHI at Florida, Bergen

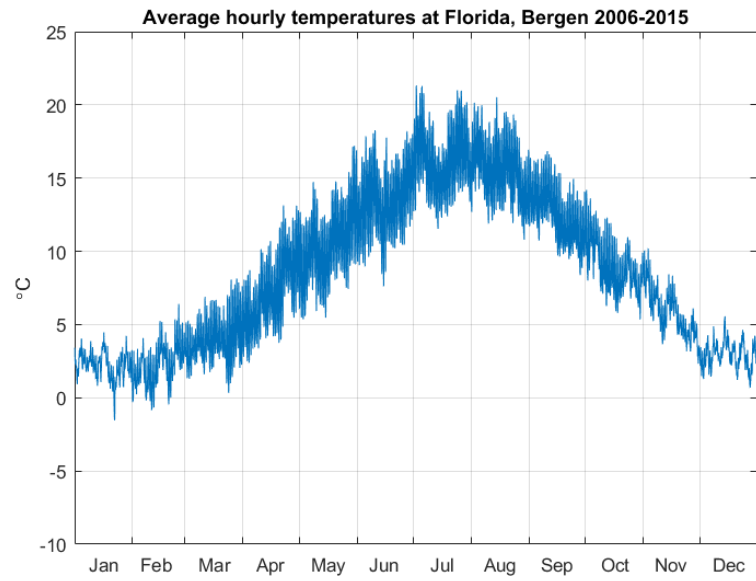
	Meas. GHI	Missing	Meas. DHI	Missing	Meteo GHI	Meteo DHI	SSE GHI	SSE DHI
Jan	6.4	0.3%	5.2	0.4%	6.4	5.2	9.0	6.8
Feb	19.8	2.3%	12.5	2.3%	20.0	14.6	26.3	17.1
Mar	51.0	1.1%	29.8	1.2%	51.1	28.9	61.1	38.4
Apr	91.3	0.9%	48.6	0.9%	90.9	55.7	108.6	59.1
May	132.3	1.2%	64.5	1.4%	141.2	72.3	162.8	76.9
Jun	140.0	1.8%	68.9	2.7%	141.4	73.1	164.7	82.8
Jul	128.8	0.6%	69.8	0.7%	127.7	81.2	152.8	80.9
Aug	100.0	1.6%	55.6	1.6%	102.6	59.4	122.5	68.5
Sep	56.3	1.1%	33.5	1.3%	61.3	39.5	74.7	42.6
Oct	28.0	0.8%	19.6	1.0%	29.6	19.7	36.9	23.9
Nov	9.1	1.4%	7.9	2.2%	9.8	7.6	13.8	9.9
Dec	3.8	0.7%	5.0	2.1%	4.2	2.8	5.3	4.0
Year	767.1	1.1%	415.6	1.5%	786.2	460.2	938.4	510.9

Table C.3: Measured versus synthetic GHI and DHI at Fagklim, Ås

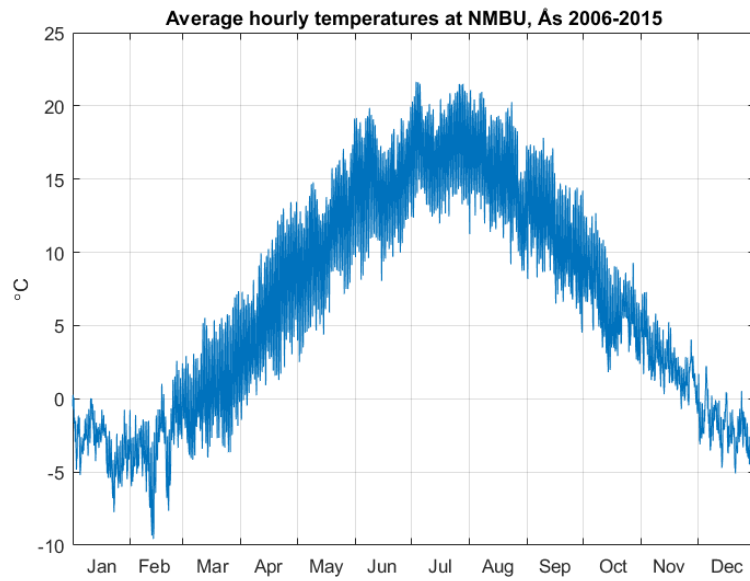
	Meas. GHI	Missing	Meas. DHI	Missing	Meteo GHI	Meteo DHI	SSE GHI	SSE DHI
Jan	9.9	-	7.5	-	8.1	5.9	12.1	8.7
Feb	24.3	-	16.8	-	22.1	14.5	30.5	19.3
Mar	70.5	-	34.0	-	67.7	33.1	71.6	41.5
Apr	113.5	-	49.1	-	110.7	54.9	111.0	59.7
May	150.7	-	67.7	-	157.5	78.0	164.9	81.5
Jun	168.5	-	71.7	-	170.7	78.5	166.2	82.8
Jul	153.0	-	71.7	-	160.2	79.5	170.8	81.2
Aug	121.2	-	56.2	3.2%	114.2	64.5	131.1	68.8
Sep	79.8	1.0%	30.9	12.9%	77.7	38.4	82.8	44.7
Oct	36.1	-	19.6	-	33.5	20.9	40.3	25.4
Nov	10.8	-	7.9	-	10.0	7.7	16.2	11.4
Dec	7.1	-	5.0	-	4.4	3.8	7.4	5.6
Year	945.3	0.1%	438.2	1.3%	936.9	479.7	1005.0	530.7



(a)



(b)



(c)

Figure C.1: Average temperatures at Trondheim, Bergen and Ås, data from eklima.met.no

Bibliography

- [1] Fraunhofer ISE, *Photovoltaics Report, updated: 6 June 2016*,
<https://www.ise.fraunhofer.de/en/downloads-englisch/pdf-files-englisch/photovoltaics-report-slides.pdf>
- [2] S. Kalogirou, *Solar Energy Engineering: Processes and Systems*, Academic Press, 2nd edition, 2014.
- [3] IEA PVPS, *Trends 2015 In Photovoltaic Applications*
http://www.iesa-pvps.org/fileadmin/dam/public/report/national/IEA-PVPS_-_Trends_2015_-_MedRes.pdf
- [4] NREL, *NREL Technique Leads to Improved Perovskite Solar Cells*
<http://www.nrel.gov/news/press/2016/36714>
- [5] M. Green et al, *Solar cell efficiency tables*, versions 1-48
- [6] PVEducation, <http://www.pveducation.org/pvcdrom/appendices/standard-solar-spectra>, retrieved september 2016
- [7] PVEducation, <http://pveducation.org/pvcdrom/2-properties-sunlight/atmospheric-effects>, retrived september 2016
- [8] NREL, <http://rredc.nrel.gov/solar/spectra/am1.5/>, retrieved september 2016
- [9] WMO Guide to Meteorological Instruments and Methods of Observation, Measurement of radiation, 2010
<http://www.wmo.int/pages/prog/www/IMOP/CIMO-Guide.html>
- [10] Newport Corporation, *Introduction to Solar Radiation*
<https://www.newport.com/t/introduction-to-solar-radiation>, retrived september 2016
- [11] HyperPhysics, *Blue Sky and Rayleigh Scattering*,

<http://hyperphysics.phy-astr.gsu.edu/hbase/atmos/blusky.html#c2>, retrieved september 2016

- [12] J. Nelson, *The Physics of Solar Cells*, Imperial College Press, 2003
- [13] W. Shockley and H. J. Queisser, *Detailed Balance Limit of Efficiency of p-n Junction Solar Cells*, *Journal of Applied Physics* volume 32, 1961
- [14] S. Rühle, *Tabulated values of the Shockley-Queisser limit for single junction solar cells*, *Solar Energy* volume 130, 2016
- [15] B. Müller et al, *On the impact of solar spectral irradiance on the yield of different PV technologies*, *Solar Energy Materials and Solar Cells*, 2015
- [16] K. Mertens, *Photovoltaics: Fundamentals, Technology and Practice*, John Wiley & Sons Ltd, 2014
- [17] R. Perez et al, *Modeling Daylight Availability and Irradiance Components From Direct and Global Irradiance*, *Solar Energy* Vol. 44, 1990
- [18] Sandia National Laboratories, *Plane of array irradiance*, <https://pvpmc.sandia.gov/modeling-steps/1-weather-design-inputs/plane-of-array-poa-irradiance/>, retrieved october 2016
- [19] Sandia National Laboratories, *Extraterrestrial radiation*, <https://pvpmc.sandia.gov/modeling-steps/1-weather-design-inputs/irradiance-and-insolation-2/extraterrestrial-radiation/>, retrieved october 2016
- [20] Ø. Holm, L. Bugge, F. Salvesen et al, *National Survey Report Norway, 2002 - 2015*, IEA-PVPS
- [21] J. Nilsen, *Norsk sol-eksplosjon*, <http://www.tu.no/artikler/norsk-sol-eksplosjon-vi-har-ristet-pa-ketchup-flasken-i-tre-ar-na-losner-det/350166>, retrieved october 2016
- [22] Ø. Byrkjedal et al, *Resource mapping of solar energy*, Kjeller Vindteknikk, 2013
- [23] Map of Meteornorm ground stations, <http://www.meteororm.com/>, retrieved october 2016
- [24] PVGIS: Computation scheme of solar radiation database, <http://re.jrc.ec.europa.eu/pvgis/solres/solrespvgis.htm>,

retrieved october 2016

- [25] I. Reda, *Improving the Accuracy of Using Pyranometers to Measure the Clear Sky Global Solar Irradiance*, NREL 1998
- [26] T. P. Chang, *The Sun's apparent position and the optimal tilt angle of a solar collector in the northern hemisphere*, Solar Energy Vol. 83, 2009
- [27] R. McCluney, *Introduction to Radiometry and Photometry*, Artech House, 1994
- [28] BenQ Solar, *SunForte PM096Boo datasheet*, http://www.benqsolar.com/download.php?file=.%2Fupload%2Fmedia%2Fbenqsolarfile%2Fdatasheet%2FSF-PM096B00_ds_en.pdf, retrieved november 2016
- [29] National Association of Norwegian Architects, *ZEB prosjekt med ambisjoner om å bli best på energi*, <http://www.arkitektur.no/haakonsvern-nytt-administrasjonsbygg-for-flo>, retrieved november 2016
- [30] IBC Solar, *MonoSol 280 ZX datasheet*, <https://shop.allnet.de/fileadmin/transfer/products/132125.pdf>, retrieved november 2016
- [31] T. Åsheim, *Solsmaragden i Drammen*, https://www.enova.no/download.aspx?OBJECT_ID=/upload_images/34C5212874974E3EBD1C5ABCBB25A839.pdf, retrieved november 2016
- [32] ISSOL sa/nv, *Solsmaragden | Union Brygge*, <http://issol.eu/solsmaragden-union-brygge-drammen/>, retrieved november 2016
- [33] J. Nilsen, *Teknisk Ukeblad, Ville kle bygget med grønne solceller – endte opp med helt ny teknologi*, <http://www.tu.no/artikler/ville-kle-bygget-med-gronne-solceller-endte-opp-med-helt-ny-teknologi/275882>, retrieved november 2016
- [34] Solar Frontier, *SF165-S datasheet*, <http://www.solar-frontier.eu/fileadmin/content/downloads/modules/en/20141030/product-overview-s-series-english.pdf>, retrieved november 2016
- [35] FutureBuilt, *Powerhouse Kjørbo: FutureBuilt forbildeprosjekt, Bærum 2014*,

- <http://www.arkitektur.no/powerhouse-kjorbo?iid=420111&pid=NAL-EcoProject-Attachments.Native-InnerFile-File>, retrieved november 2016
- [36] SunPower, *SPR-327NE-WHT-D datasheet*, http://www.nqsolar.com.au/wp-content/uploads/2013/07/SunPower_327W_E20.pdf, retrieved november 2016
- [37] J. Nilsen, Teknisk Ukeblad, *Slik kan nye matbutikker se ut om fem år*, <http://www.tu.no/artikler/slik-kan-nye-matbutikker-se-ut-om-fem-ar/276934>, retrieved november 2016
- [38] J. Hindklev, Bygg.no, *Kiwi Fjeldset*, <http://www.bygg.no/article/1266692?image=dp-image75146-1266715>, retrieved november 2016
- [39] G. H. Yordanov et al, *Extreme overirradiance events in Norway: 1.6 suns measured close to 60°N*, Solar Energy Vol. 115, 2015
- [40] M. Wolff, V. Thue-Hansen and A. A. Grimenes, *Meteorologiske data for Ås*, NMBU 2006 – 2009
- [41] NMBU, *Instrumenter - Energi og stråling*, <https://www.nmbu.no/fakultet/realtek/laboratorier/fagklim/male-instrumenter/straling>, retrieved november 2016
- [42] S. Otterlei, NRK, *Ny nedbørsrekord i Bergen*, <https://www.nrk.no/hordaland/ny-nedborsrekord-i-bergen-1.13063470>, retrieved december 2016
- [43] M. Hirth, Sysla Grønn, *Her får kyrne strøm fra solen*, http://syslagronn.no/2016/03/31/syslagronn/her-far-kyrne-strom-fra-solen_85573/, retrieved december 2016
- [44] Sandia National Laboratories, *Isotropic Sky Diffuse Model*, <https://pvpmc.sandia.gov/modeling-steps/1-weather-design-inputs/plane-of-array-poa-irradiance/calculating-poa-irradiance/poa-sky-diffuse/isotropic-sky-diffuse-model/>, retrieved december 2016
- [45] Sandia National Laboratories, *Hay and Davies Sky Diffuse Model*, <https://pvpmc.sandia.gov/modeling-steps/1-weather-design-inputs/plane-of-array-poa-irradiance/calculating-poa-irradiance/poa-sky-diffuse/hay-sky-diffuse-model/>, retrieved december 2016

- [46] J. Olseth and A. Skartveit, *Modelling Slope Irradiance at High Latitudes*, Solar Energy Vol. 36, 1986
- [47] A. Virtuani et al, *Overview of Temperature Coefficients of Different Types of Thin Film Photovoltaic Technologies*, 25th EU-PVSEC Conference, 2010
- [48] N. H. Reich et al, *Weak Light Performance and Spectral Response of Different Solar Cell Types*, EGN Solar Energy, 2005
- [49] Solar Frontier, *CIS PowerModules by Solar Frontier*, http://www.solar-frontier.eu/fileadmin/content/downloads/powermodule/20150609/CIS-Broschuere_EN_PowerModules.pdf, retrieved december 2016
- [50] M. Gostein and L. Dunn, *Light Soaking Effects on PV Modules: Overview and Literature Review*, https://www1.eere.energy.gov/solar/pdfs/pvmrw2011_p25_tf_dunn.pdf, retrieved december 2016
- [51] The Norwegian Solar Energy Society, *Bruk av solenergi i Norge*, http://solenergi.no/wp-content/uploads/2010/01/Solguiden_A6_enkeltsider_okt15-2.pdf, retrieved december 2016
- [52] T. Ericson and H. Halvorsen, *SSB Hvordan varierer timeforbruket av strøm i ulike sektorer?*, Økonomiske Analyser 6/2008
- [53] G. Janssen et al, *Outdoor Performance of the Bifacial Module*, Energy Procedia 77, 2015
- [54] J. Singh et al, *Performance Investigation of Bifacial PV Modules in the Tropics*, 27th EU PVSEC, 2012
- [55] JRC Renewable Energies Unit, *PVGIS radiation databases*, http://re.jrc.ec.europa.eu/pvgis/apps4/databasehelp_en.html, retrieved december 2016
- [56] JRC Renewable Energies Unit, *Frequently Asked Questions about PVGIS and Interactive Maps*, <http://re.jrc.ec.europa.eu/pvgis/info/faq.htm>, retrieved december 2016
- [57] PVsyst 6 Help, *NASA-SSE data*, http://files.pvsyst.com/help/meteo_source_nasa.htm, retrieved december 2016

- [58] PVsyst 6 Help, *Meteonorm data and program*,
http://files.pvsyst.com/help/meteo_source_meteonorm.htm, retrieved december 2016
- [59] B. Liu and R. Jordan, *The Interrelationship and Characteristic Distribution of Direct, Diffuse and Total Solar Radiation*, Solar Energy Vol. 4, 1960
- [60] PVsyst 6 Help, *Diffuse Irradiance model*,
http://files.pvsyst.com/help/meteo_diffuse.htm, retrieved december 2016
- [61] PVsyst 6 Help, *Sandia Model for PV modules*,
http://files.pvsyst.com/help/sandia_model.htm, retrieved december 2016
- [62] A. Mermoud, PVsyst forums, *How does PVsyst take the spectral effect into account?*,
<http://forum.pvsyst.com/viewtopic.php?f=19&t=266>, retrieved december 2016
- [63] PVsyst 6 Help, *Array Thermal losses*,
http://files.pvsyst.com/help/thermal_loss.htm, retrieved december 2016
- [64] PVsyst 6 Help, *Array incidence loss (IAM)*,
http://files.pvsyst.com/help/iam_loss.htm, retrieved december 2016
- [65] O. M. Midtgård et al, *A qualitative examination of performance and energy yield of photovoltaic modules in southern Norway*, Renewable Energy Vol. 35, 2010
- [66] A. G. Imenes et al, *Development of a Test Station for Accurate In Situ I-V Curve Measurements of Photovoltaic Modules in Southern Norway*, Conference Record of the IEEE Photovoltaic Specialists Conference, 2011
- [67] T. A. Brekke, *Nordic Irradiance Conditions and the Effects on Solar Module Efficiency*, NMBU Master's Thesis, 2016
- [68] D. Verma et al, *Outdoor Performance of North-Facing Multicrystalline Modules in Southern Norway*, Photovoltaic Specialists Conference (PVSC), 2012 38th IEEE
- [69] C. Good et al, *Solar Cells Above the Arctic Circle – a Comparison Between*

- a Two-Axis Tracking System and Simulations*, 24th European Photovoltaic Solar Energy Conference (EUPVSEC), 2009
- [70] A. G. Imenes et al, *Field stations in Norway and Kenya for comparative analysis of compensated and standard SoG polysilicon modules*, 25th European Photovoltaic Solar Energy Conference, 2010
- [71] B. Thorud and S. Merlet, *Solenergi i Norge: Status og framtidsutsikter, Hva betyr solenergirevolusjonen?*, Norsk Klimastiftelse, 2015
- [72] Norges vassdrags- og energidirektorat, *Vannkraftpotensialet*, <https://www.nve.no/energiforsyning-og-konsesjon/vannkraft/vannkraftpotensialet/>, retrieved december 2016
- [73] Eurostat, *Electricity price statistics*, [http://ec.europa.eu/eurostat/statistics-explained/index.php/File:Half-yearly_electricity_and_gas_prices_\(EUR\).png](http://ec.europa.eu/eurostat/statistics-explained/index.php/File:Half-yearly_electricity_and_gas_prices_(EUR).png), retrieved december 2016
- [74] Oslo kommune, *Støtte til installering av solceller*, <http://oslosola.no/stotte.html>, retrieved december 2016
- [75] Enova SF, *Tilskudd for el-produksjon*, <https://www.enova.no/finansiering/privat/enovatilskuddet/el-produksjon/tilskudd-for-el-produksjon/914/1981/>, retrieved december 2016
- [76] R. Gottschalg et al, *Experimental study of variations of the solar spectrum of relevance to thin film solar cells*, Solar Energy Materials and Solar Cells Vol. 73, 2003
- [77] PVsyst 6 Help, *LID (Light Induced Degradation) Loss*, http://files.pvsyst.com/help/lid_loss.htm, retrieved december 2016

